國 立 交 通 大 學

材 料 科 學 與 工 程 學 系
奈 米 科 技 碩 士 班

碩 士 論 文

結合雙股去氧核醣核酸之磁性氧化鐵-金核殼奈米粒子的合成及特性分析用於可調節藥物釋放系統之研究

Synthesis and Characterization of Double Strand DNA-Conjugated Magnetic Fe_3O_4 Core/Au Shell Nanoparticles for a Tunable Drug Delivery System

研 究 生 ： 林庭仔　　**Ting–Yu Lin**

指導教授 ： 柯富祥 教授　**Prof. Fu–Hsiang Ko**

中 華 民 國 一 〇 一 年 八 月

結合雙股去氧核醣核酸之磁性氧化鐵-金核殼奈米粒子的合成及特性分析用於可調節藥物釋放系統之研究

Synthesis and Characterization of Double Strand DNA-Conjugated Magnetic Fe_3O_4 Core/Au Shell Nanoparticles for a Tunable Drug Delivery System

研 究 生：林庭仔　　Student：Ting-Yu Lin

指導教授：柯富祥 教授　　Advisor：Prof. Fu-Hsiang Ko

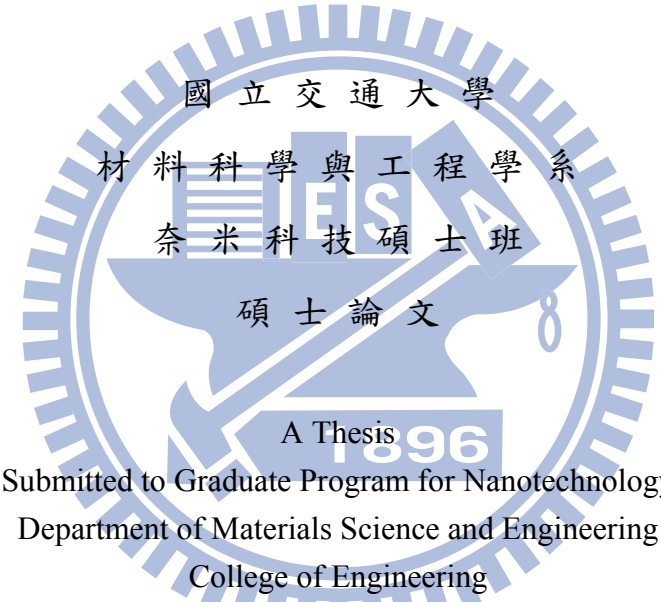

國 立 交 通 大 學

材 料 科 學 與 工 程 學 系

奈 米 科 技 碩 士 班

碩 士 論 文

A Thesis

Submitted to Graduate Program for Nanotechnology

Department of Materials Science and Engineering

College of Engineering

National Chiao Tung University

in partial Fulfillment of the Requirements

for the Degree of

Master

in

Nanotechnology

August 2012

Hsinchu, Taiwan, Republic of China

中華民國一〇一年八月

結合雙股去氧核醣核酸之磁性氧化鐵-金核殼奈米粒子的合成及特性分析用於可調節藥物釋放系統之研究

研究生:林庭伃　　指導教授:柯富祥 教授

國立交通大學材料科學與工程學系 奈米科技碩士班

摘 要

殼核雙金屬奈米粒子由兩種不同的材質所組成，與單一成分奈米粒子受限於單一性質相比，其更具新穎性及功能性。本篇研究以共沉澱法製備具良好分散性之奈米氧化鐵粒子，隨後以還原法在粒子表面沉積金殼層。並以穿透式電子顯微鏡以及選區電子繞射圖證實氧化鐵-金奈米粒子之核殼結構。此外，由紫外光-可見光吸收光譜以及超導量子干涉儀之量測，可證明氧化鐵-金奈米粒子具有金殼層之光學性質及氧化鐵核之超順磁特性。由於金殼層表面可與修飾有硫基的雙股去氧核醣核酸分子(DNA)作有效結合；同時利用一具有螢光特性的抗癌藥物「小紅莓」，可嵌入經設計的雙股去氧核醣核酸連續且重複的CG鹼基中，形成一創新且多功能的藥物載體。進一步地，將此磁性氧化鐵-金核殼奈米載體置於射頻磁場下，其磁性氧化鐵核因感應磁場而產生熱能，使得對熱敏感的雙股去氧核醣核酸解旋進而在短時間內釋放出藥物小紅莓。而藉由調整射頻磁場開啟的時間，便能調控藥物釋放的量。在本研究中，利用此一藥物釋放系統，在10分鐘內即可達到79%的釋放率。

未來，此載體仍具有巨大發展潛力。金殼層表面可修飾專一性辨識分子的便利性，以及磁性氧化鐵核具有核磁共振顯影能力，加之無論是金或是氧化鐵，都已有文獻指出其高度生物相容性。假以時日，可使此磁性氧化鐵-金核殼奈米粒

子的藥物釋放系統成為同時具有顯影能力、標靶治療，並且能調控藥物釋放的完整生醫奈米操作平台。

Synthesis and Characterization of Double Strand DNA-Conjugated Magnetic Fe_3O_4 Core/Au Shell Nanoparticles for a Tunable Drug Delivery System

Student: Ting–Yu Lin Advisor: Prof. Fu–Hsiang Ko

Institute of Nanotechnology

National Chiao Tung University

Abstract

Magnetic Fe_3O_4 core/Au shell nanoparticles exhibit both magnetic property of Fe_3O_4 core and well-established surface chemistry, biological reactivity of Au shell. In this study, magnetic Fe_3O_4 core/Au shell nanoparticles were synthesized by reducing $HAuCl_4$ on the surface of monodispersed Fe_3O_4 nanoparticles in the aqueous solution after the facile synthesis of Fe_3O_4 nanoparticles by co-precipitation process that are more popular for biological applications. Next, transmission electron microscopy (TEM) images, selected-area electron diffraction (SAED) patterns, and optical property by UV-Vis all clearly demonstrate the fact that core/shell nanoparticles were successfully formed as the form of Fe_3O_4 nanoparticles covered by Au shell; as well as superconducting quantum interference device (SQUID) results show the great superparamagnetic property of Fe_3O_4 core/Au shell nanoparticles. In addition, by functionalizing the surfaces of magnetic Fe_3O_4 core/Au shell nanoparticles with CG rich double strand DNA through Au-S bonds, which are thermo-sensitive molecules, the doxorubicin with fluorescence as anticancer drug

could be carried via intercalation. Further, when the innovative drug carriers were heated under high frequency magnetic field, the double strand DNA dehybridized and then caused the release of doxorubicin. Among suffered different periods of high frequency magnetic field, the release of doxorubicin can be tuned. In this study, the release rate can achieve up to 79% in less than 10 minutes based on our drug delivery system.

As a result, this tunable drug delivery system with magnetic Fe_3O_4 core/Au shell carriers has great promising of developing into multifunctional system including imaging, targeting and tunable drug delivery owing to not only the potential in MR imaging of magnetic core but also well-established surface with adaptive targeting molecules of Au shell, even the proved biocompatibility whether it is Au or Fe_3O_4 nanoparticle. In the future, a complete bionano platform will be built up.

Key words: magnetic, core/shell, nanoparticles, drug delivery, doxorubicin

Acknowledgment

感謝柯富祥教授在學生的碩士生涯期間給予最充分的指導，並且提供豐富的資源與安全的實驗室環境，使我們能專心致志於研究以完成本篇論文。謝謝系主任陳三元教授與其實驗室的同學，提供高週波加熱器以及磁學上的指導。

謝謝所有屬於柯富祥老師實驗室的學長姐、同學、學弟妹，不管是已經畢業或者是陪我一起度過碩班兩年生活，因為有你們當初的努力，才有今日的後人乘涼；因為有你們在實驗與報告上的指導與建議，才有我今日的進步；因為有你們平時的陪伴與關心，才使我的生活多彩多姿。

最後感謝我最親愛的家人與朋友一路的陪伴與支持，在日常生活中關心我，在我遇到挫折時給予我鼓勵，使我可以無後顧之憂的完成碩班的學業，謝謝你們!

Contents

List of Tables

List of Figures

reporters (optical, radio, magnetic), and potential therapeutic payloads (gene, radio, chemo). (B) Four possible modes of action for various therapeutic agents; a) Specific MNP binding to cell surface receptors (i.e. enzymes/proteins) facilitate their internalization and/or inactivation, b) controlled intercellular release of chemotherapeutics; c) release of gene therapeutic materials post endosomal escape and subsequent targeting of nucleus; and d) intracellular decay of radioactive materials.[30]

Illustration of the two components of the magnetic relaxation of a magnetic fluid.[51]

Absorption (a) and photoluminescence (b) spectra of CdSe core and CdSe/ZnSe core/shell nanocrystals before (dashed lines, toluene solutions) and after (solid lines, aqueous solutions) functionalization with MUA. All colloidal solutions exhibit identical optical densities at the first exciton absorption peak.[52]

(A) Mercaptoalkyl-oligonuleotide-modified Ag core/Au shell particles and polynucleotide target. DNA spot test using: (B) 12.4 nm Ag/Au nanoparticle probes and (C) 13 nm Au nanoparticle probes: (I) without target, (II) with target at room temperature, (III) with target at 58.0°C, a temperature above the T_m (53.0°C) of the hybridized DNA.[53]

Thiol and carboxy modified γ-Fe_2O_3 beads are reacted with CdSe/ZnS QDs to form the luminescent/magnetic nanocomposite particles.[54]

Chapter 1: Introduction

1.1 General Introduction

"There's plenty of room at the bottom," an invitation to enter a new field of physics, is the title of a classic speech given by the great physicist Richard Feynman at the annual meeting of the American Physical Society at the California Institute of Technology on December 29, 1959. Over 40 years ago, Feynman considered a new physical world of ultra-small volumes and highlighted some difficulties that researchers might confront when visiting it. His speech provided a vision for scientists and engineers to establish a new field, which—with subsequent developments in novel manufacturing skills and equipment—is now known as "nanotechnology."

Nanotechnology has become one of the most important and interesting forefront field in physics, chemistry, biology and engineering which the characteristic dimensions are below ca. 1000 nm in recent years. It shows grand promise for providing us in the near future with numerous breakthroughs that will change the progress of technological advances in a wide range of applications. This kind of work is often referred to as nanotechnology.

1.2 Nanomaterials

An atom measures about 1 Å, or 10^{-10} meters. The study of atoms and molecules is the traditional field of chemistry as was researched in the late 19th and 20th centuries. A nanometer (nm), or 10^{-9} meters, represent a collection of small number atoms or molecules. Properties of bulk substances of micrometer sizes or larger have been researched for years by solid state physicists and material scientists and are currently well understood. Materials on the 1-100 nm scale were not studied by either

group in the past. It was just recently shown that on this size scale the properties of a material become dependent on its shape and size. Therefore, the nanometer scale incorporates collections of molecules or atoms, whose properties are neither those of the bulk nor those of the individual components. On this scale, numerous atoms are still situated on the surface, or one layer removed from the surface, rather than the interior. Different properties are seen on this scale due to the interface that is not seen in the bulk or individual atom. Since the properties depend on the size of the structure, instead of the nature of the material, continual and reliable change can be realized using a single material.[1]

As the size reducing to the nano-regeime, a variety of properties different from the bulk emerge, including optical, thermal, magnetic, and mechanical properties were shown. The optical properties such as light absorption or microwave absorption are significantly increased, and the absorption peak of Plasmon Resonance shifted which creates the new optical character, such as infrared absorption and emission but a sheltered role in ultraviolet, as well as the different size of metal particles with distinct light-scattering properties (Figure 1.1).

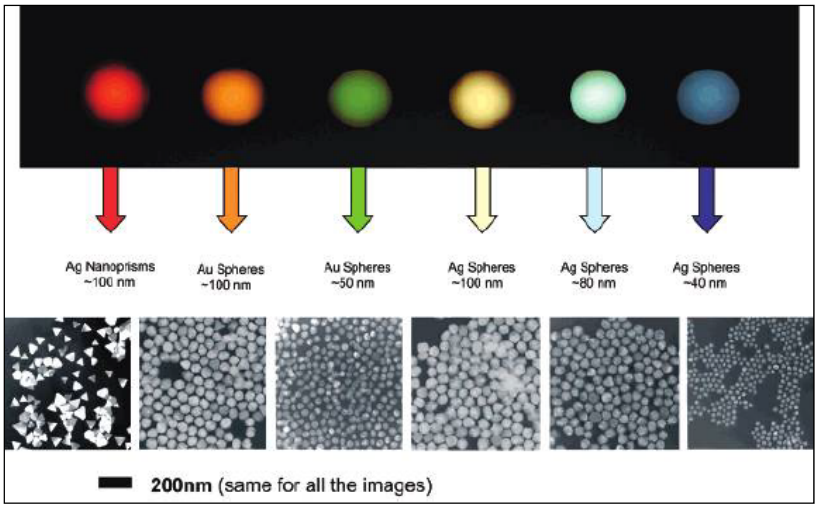

Figure 1.1 Sizes, shapes, and compositions of metal nanoparticles can be systematically varied to produce materials with distinct light-scattering properties.[2]

Nanoparticles have small thermal resistance and excellent thermal conductivity at low temperature, and can be used as a low-temperature thermal conductivity of materials, because the amplitude of the nanomaterials surface atoms is twice as much as the internal atoms. With the particle size decreases, the proportion of surface atoms is gradually increased, and the melting point of nanomaterials will reduce, distinguished the thermal properties. Moreover, when a magnetic material size decreased, its magnetic susceptibility with decreasing temperature is gradually reduced. The magnetically ordered state turns into a magnetic disordered state, and the superconducting phase transfers to the normal phase; therefore some new magnetic properties will generate (Figure 1.2). In addition, the strength, wear resistance, aging resistance, pressure resistance, toughness, tight and waterproof characteristic of nanocomposites are greatly increased and improved due to the inadequate coordination surface atoms coupling with a very strong van der Walls fore. Thus, some different mechanical properties are exhibited.

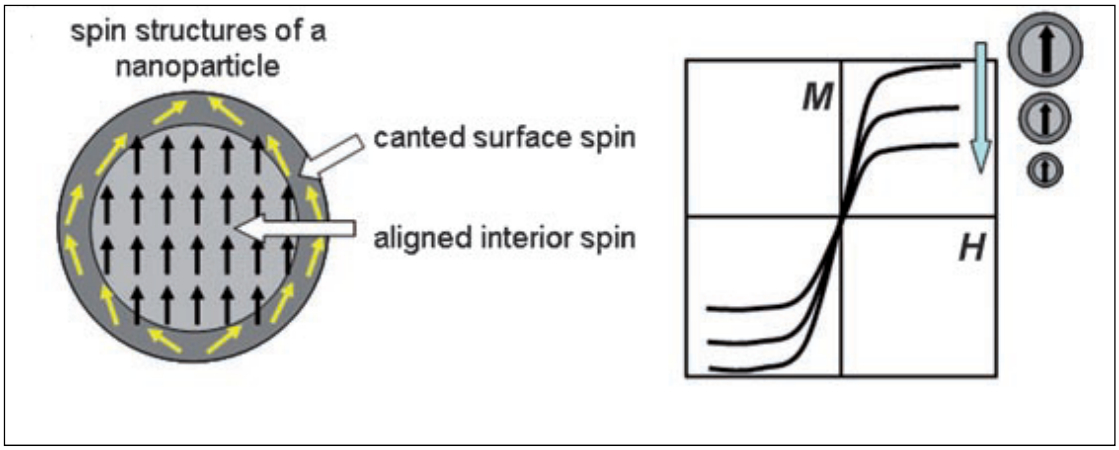

Figure 1.2 Surface spin canting effect of a nanoparticle upon magnetization (M magnetic moment, H external magnetic field).[3]

Besides, there are some physical effects appeared when the materials reduced to nano size, making several properties different from the bulk materials such as the light absorption, coercive force and melting point, called small size effect. The surface atom of nanomaterials is increased, which makes high ratio of surface-to-volume, and increases the surface energy, which was known as surface effect. Quantum size effect occurs when the valence band and energy band gap of metal or semiconductor nanomaterials widen which induce the insulation. Some nanoparticles having the ability to run through the energy barrier is quantum tunneling effect. And some nanomaterials show coulomb blockade effect, such as metal and semiconductor showing that the charge and discharge process is not a continuous effect. In other words, the current with the voltage increase is no longer straight up, but stepped up. Along with synthetic advances for varying the composition, shape, and size of nanostructured materials has come the most competitive candidate in various applications.

1.3 Nanobiotechnology

Nanomaterials, such as semiconductor or metal nanorod and nanoparicles, show similar dimensions to those of biomolecules, such as DNA or RNA or proteins. Both materials science and biotechnology meet at the same length scale (Figure 1.3). On one hand, biomolecular constituents have typical size dimensions in the range of about 5 to 200 nm; on the other hand, commercial requirements to produce increasingly miniaturized microelectronic devices strongly motivate the elaboration of nanoscale systems. Today's nanotechnology research puts a grand importance on the development of bottom-up strategies, which interest the self-assembly of (macro) molecular and colloidal building blocks to create larger, functional devices.

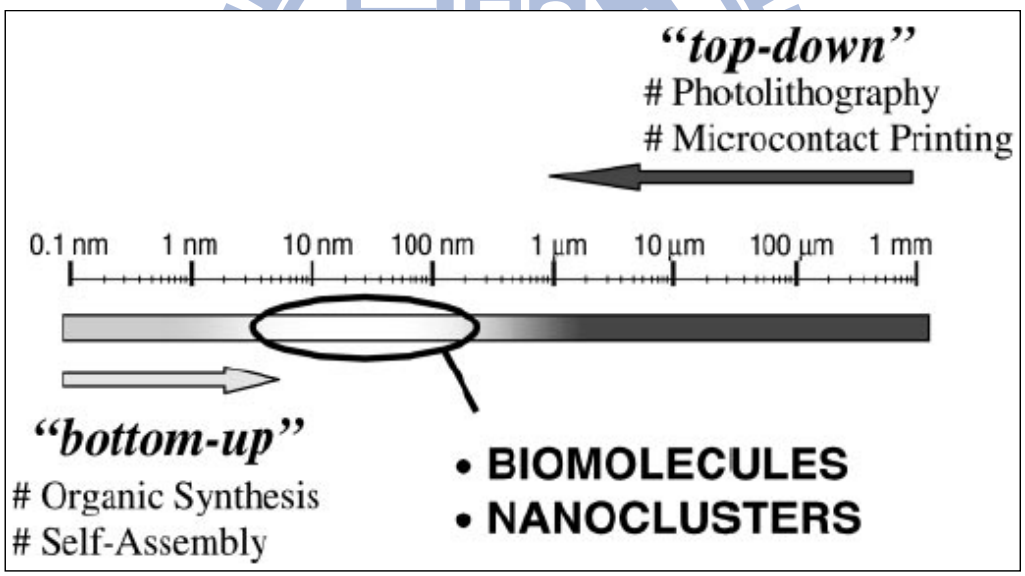

Figure 1.3 A gap currently exists in the engineering of small-scale devices. Whereas conventional top-down processes hardly allow the production of structures smaller than about 200±100 nm, the limits of regular bottom-up processes are in the range of about 2±5 nm.[4]

The combination of nanomaterials and biotechnology has led to the development of the hybrid nanomaterials that combine the highly selective catalytic and

recognition properties of biomaterials, such as DNA and protein/enzymes, with unique photonic, electronic, and catalytic features of nanoparticles. Because of many fundamental features, biomaterials are major future building blocks for nanomaterials architectures. Biomaterials play the roles of specific and strong complementary recognition interactions, for example, nucleic acid–DNA antigen–antibody, and hormone–receptor interactions. The functionalization of nanomaterials with biomolecules could lead to biomolecule-nanoparticle recognition interactions and thus to self-assembly. In addition, numerous biomolecules contain several binding sites. First, for example, antibodies show two Fab (antigen-binding fragment) sites, whereas streptavidin or concanavalin A each exhibit four binding domains. This allows the multidirectional growth of nanomaterial structures. Second, proteins may be genetically engineered and modified with specific anchoring groups. This assists their aligned binding to nanomaterials or the site-specific linkage of the biomaterial to surfaces. As the result, the directional growth of nanomaterial structures may be instructed. Furthermore, other biomolecules, such as double-stranded DNA, may be synthetically produced in complex rigidified structures that play the role of templates for the assembly of nanomaterials by intercalation, electrostatic binding to phosphate groups, or association to functionalities tethered to the DNA. Next, enzymes are catalytic instruments for the manipulation of biomaterials. For example, the endonuclease scission processes of nucleic acids or the ligation provide effective instruments for controlling the structure and shape of biomolecule-nanomaterial hybrid systems. In this context, it is important to notice that Mother Nature has processed unique biocatalytic replication developments. The use of biocatalysts for the replication of biomolecule-nanomaterial conjugates may provide a productive system for the production of nanostructures of predesigned compositions and shapes.[5-6] In this regard, the conjugation of nanomaterials (e.g. nanoparticles,

nanorods, nanowires) with biomolecules (e.g. DNA, RNA, proteins) is a desirable area of research within nanobiotechnology.

Biomolecule-functionalized nanomaterials could be exploited for abundant applications in biomolecular biosensors,[7-8] immunoassays,[9] medicine,[10] and electronics,[11-12] namely in drug delivery,[13] photodynamic anticancer therapy, electronic DNA sequencing, targeted delivery of radioisotopes, gene therapy, and nanotechnology of gene-delivery systems in Figure 1.4. Novel fascinating regions of technologies are practical with the use of bionanomaterials. A combination of the unique properties of biomaterials and nanomaterials provides a unique chance for chemists, physicists, biologists, and material scientists to shape the new region of nanobiotechnology.[14] Based on recent progress in the field, invigorating new science and novel system can be anticipated from the interdisciplinary effort. Future progress will need continued innovation by nanotechnology in close cooperation with experts in biological and medical fields.

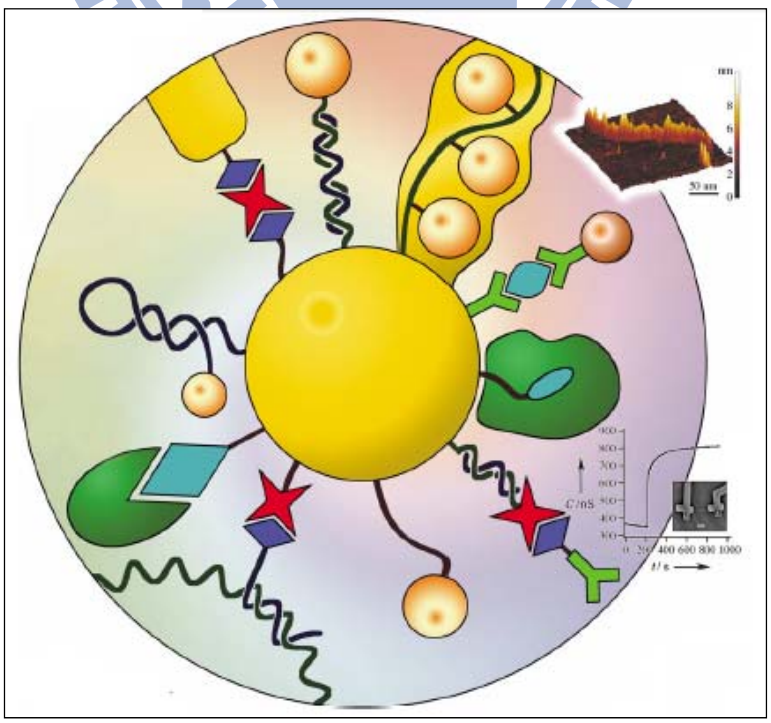

Figure 1.4 Integrated nanoparticle–biomolecule hybrid systems.[5]

Chapter 2: Literatures Review & Motivation

2.1 Applications of Fe_3O_4 Superparamagnetic Nanoparticles

Superparamagnetic Fe_3O_4 nanoparticle with proper surface chemistry have been extensively used for several *in vivo* applications, such as drug delivery, cell separation, immunoassay, tissue repair, detoxification of biological fluids, and magnetic resonance (MR) imaging contrast enhancement (Figure 2.1).[15] Because of its unique characters including degradable innocuously, manipulated by an external magnetic field, and heated by high frequency magnetic fields, which is called hyperthermia. It is notable that all of these bioengineering and biomedical applications require that the nanoparticles have a narrow particle size distribution, a size smaller than 100 nm, and high magnetization values, so that the nanoparticles have uniform chemical and physical properties.

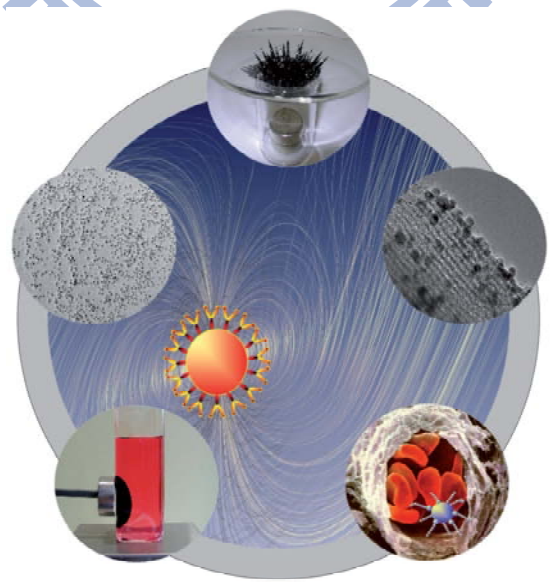

Figure 2.1 Magnetic nanoparticles: synthesis, protection, functionalization, and application.[16]

There are several popular methods to synthesize monodispersed, highly stable, and shape-controlled magnetic nanoparticles, including co-precipitation, thermal decomposition, microemulsion, and hydrothermal synthesis. There follows each method respectively.

Co-precipitation is a convenient and facile way to synthesize Fe_3O_4 nanoparticles, which prepared under atmosphere at room temperature. The chemical reaction of Fe_3O_4 co-precipitation is given in Figure 2.2. By modulating type of salt used, reaction temperature, Fe^{2+}/Fe^{3+} ratio, ionic strength of the media, and pH value, different shape, size, and composition of magnetic nanoparticles are altered.[17] However, nanoparticles synthesized by this method tend to be rather polydispersed.

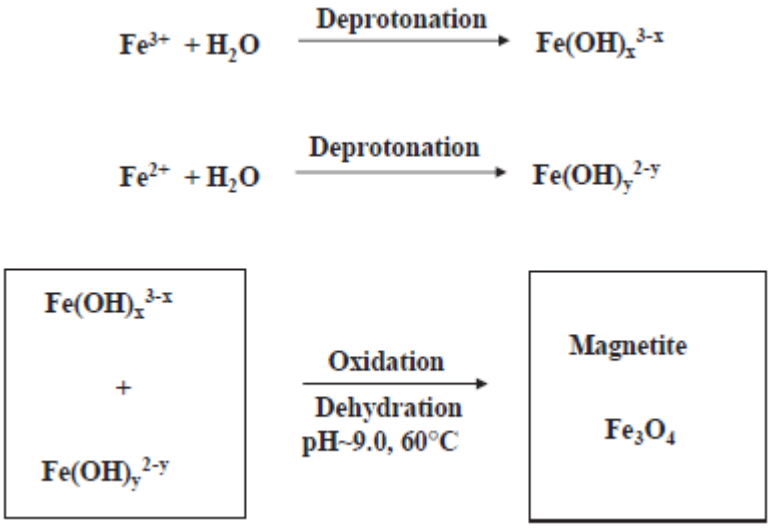

Figure 2.2 The reaction mechanism of Fe_3O_4 particle formation from an aqueous mixture of ferrous and ferric chloride by addition of a base.[17]

Fe_3O_4 nanoparticles by thermal decomposition synthesized are usually synthesized with a narrow size through the organometallic compounds in high-boiling organic solvents with stabilizing surfactants (Figure 2.3).[18-19] The reaction temperature, aging period, and the ration of the starting reagents are the determining

parameters for the control of the morphology and the size of magnetic nanoparticles. The reactivity was tuned by altering the concentration and the chain length of fatty acids. However, it is unclear whether the magnetic nanoparticles can be dispersed in water, so the water-soluble magnetic nanoparticles are more popular for biological applications.

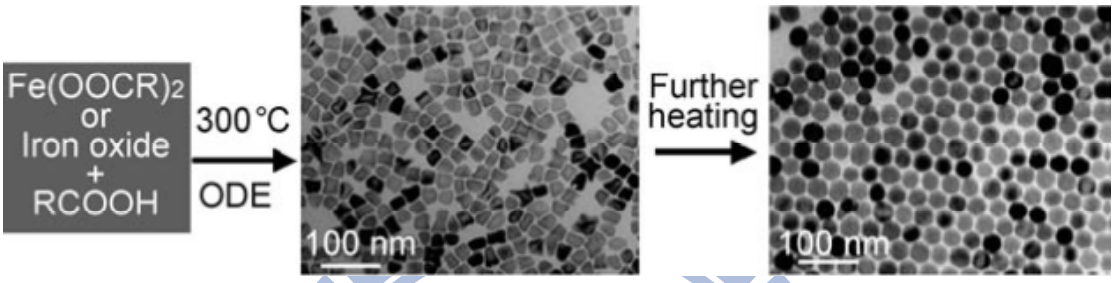

Figure 2.3 The formation of Fe_3O_4 nanocrystals. The middle and right panels are TEM images of the as-synthesized nanocrystals taken at different reaction times.[20]

In addition to the above-mentioned two methods, microemulsion is a thermodynamically stable isotropic dispersion of two immiscible liquids, where the microdomain of either or both liquids has been stabilized by an interfacial film of surfactant molecules. Nevertheless, the shape and size of the Fe_3O_4 nanoparticles usually vary over a relatively wide range.[21]

Hydrothermal synthesis is a liquid-solid-solution reaction which is more complicated and expensive. During reaction process, a variety of different nanocrystals have been synthesized. This system consists of solid (metal linoleate), a liquid phase (ethanol-linoleic acid), and a solution (water-ethanol) at different reaction temperatures under hydrothermal conditions (Figure 2.4).[22] In this way, Fe_3O_4 nanopaeticles were obtained with adjustable sizes in the range of 200-800 nm. In the following, Table 2.1 shows the comparison of the advantages and disadvantages of the four above-mentioned methods.

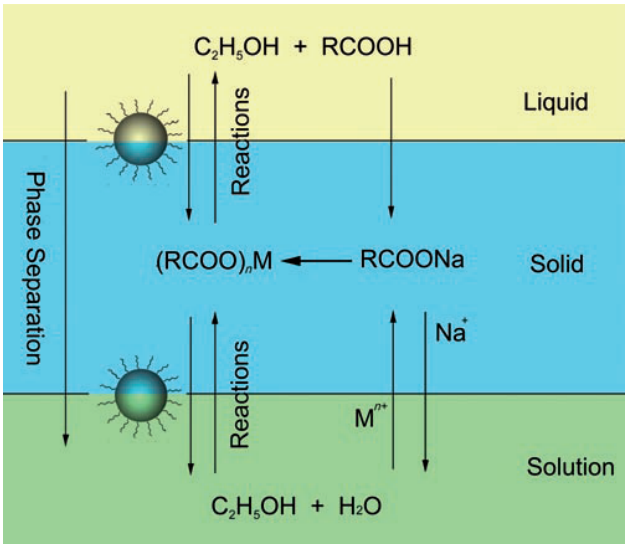

Figure 2.4 The liduid-solid-solution (LSS) phase transfer synthetic strategy.[22]

Synthetic method	Synthesis	Reaction temp. [°C]	Reaction period	Solvent	Surface-capping agents	Size distribution	Shape control	Yield
co-precipitation	very simple, ambient conditions	20–90	minutes	water	needed, added during or after reaction	relatively narrow	not good	high/ scalable
thermal decomposition	complicated, inert atmosphere	100–320	hours–days	organic compound	needed, added during reaction	very narrow	very good	high/ scalable
microemulsion	complicated, ambient conditions	20–50	hours	organic compound	needed, added during reaction	relatively narrow	good	low
hydrothermal synthesis	simple, high pressure	220	hours ca. days	water-ethanol	needed, added during reaction	very narrow	very good	medium

Table 2.1 Summary comparison of Fe_3O_4 nanoparticles synthetic methods.[16]

The stability of Fe_3O_4 nanoparticles is important for the preparation and storage. With appropriate surface coating, Fe_3O_4 nanoparticles can be dispersed into suitable solvents, forming ferrofluids. Nanosized particles have chemical and physical properties that are characteristic of neither the bulk nor the atom.[23] The large surface area and quantum size effects of Fe_3O_4 nanoparticles dramatically alter some of the magnetic properties and show superparamagnetic phenomena, because each particle can be seen as a single magnetic domain.[24] Based on their unique nature, Fe_3O_4 superparamagnetic nanoparticles have been widely used in biological applications.

2.1.1 Magnetic Resonance Imaging

Magnetic resonance (MR) imaging is one of the greatest non-invasive imaging modalities used in clinical medicine today, which based on the property that hydrogen protons will align and process around an applied magnetic field, B_0. Upon applying a transverse radiofrequency (rf) pulse, the protons are perturbed from B_0. The following process through which the protons return to their original state is called the relaxation phenomenon. There are two independent process, longitudinal relaxation (T_1) and transverse relaxation (T_2), which can be monitored to create an MR imaging. The local variation of relaxation is corresponding to imaging contrast, which arises from proton density as well as the physical and chemical properties of the tissues.[25]

Superparamagnetic nanoparticles play a magnificent role as MR imaging contrast agents, to better distinguish healthy and pathological tissues. Under an applied B_0, superparamagnetic nanoparticles induce a magnetic dipole moment μ. When water molecules diffuse into the periphery of the induced μ, the magnetic relaxation processes of the water protons are perturbed and T_2 is shorted, which result in the darkening of the corresponding area in T_2-weighted MR imaging (Figure 2.5). The degree of the T_2 contrast effect is illustrated by the spin-spin relaxivity R_2 ($1/T_2$). The higher values of R_2 result in a better contrast effect.

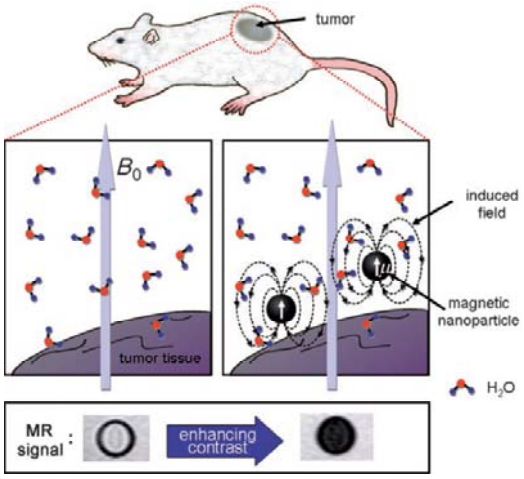

Figure 2.5 MR contrast effect of magnetic nanoparticles (MNPs). Under an external field B_0, MNPs are magnetized with a magnetic moment of μ and generate an induced magnetic field which perturbs the nuclear spin relaxation processes of the water protons. This perturbation leads to MR contrast enhancement which appears as a darkening of the corresponding section of the image.[26]

The control of nanoparticle magnetism should be led to a maximum R_2 value. Therefore, by modulating the nanoparticle parameters, synthetic magnetic nanoparticles can be designed and constructed to raise the MR contrast-enhancement effects (Figure 2.6). Moreover, controlling the magnetic core, modifying the ligand shell to reach high colloidal stability and biocompatibility, and conjugating the biomolecules to get the molecular targeting capability, can make the nanoparticles for MR imaging of cancer, cellular trafficking, angiogensis, and therapy (Figure 2.7).[26]

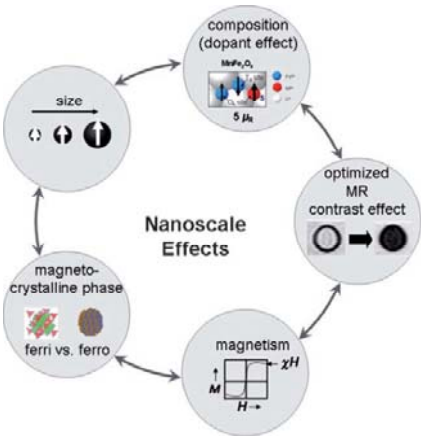

Figure 2.6 Important parameters of MNPs for MR contrast-enhancement effects.[26]

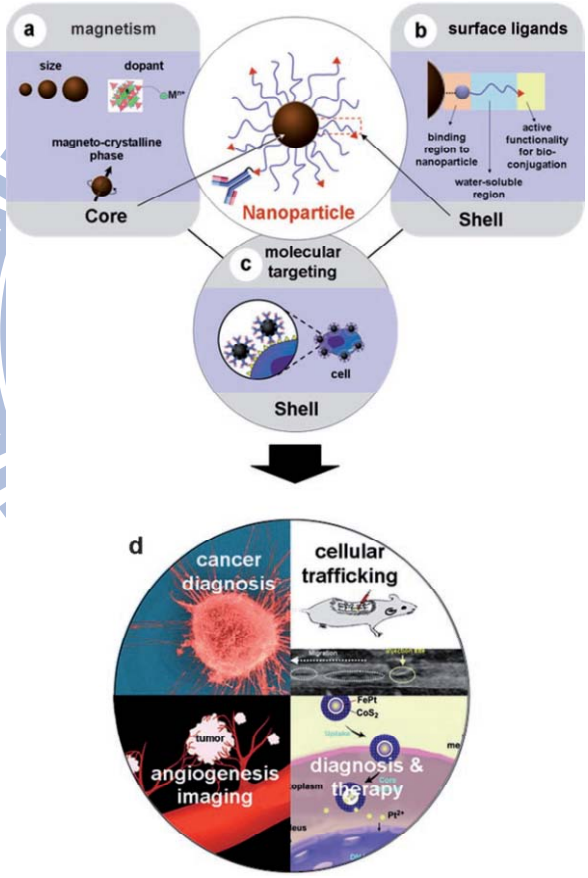

Figure 2.7 Tailored MNPs for molecular and cellular MR imaging. (a) Controlling the magnetism of the nanoparticle core, (b) tailoring the surface ligands of the nanoparticle shell and (c) the molecular targeting capability of biomolecule-conjugated nanoparticles. (d) High performance utilizations of nanoparticles for molecular and cellular MR imaging.[26]

2.1.2 Drug Delivery

Another possible and most favorable application of Fe_3O_4 nanoparticles is in drug delivery as vehicle of therapeutic drug for targeting delivery. When packing a therapeutic drug and with a proper design, Fe_3O_4 nanoparticles can act as efficient drug delivery systems, which offer a variety of drug loaded, control the drug release, and track the delivery by using Fe_3O_4 nanoparticles imaging modality. There are several factors, such as the size, charge and surface chemistry of Fe_3O_4 nanoparticles, particularly and strongly affect both the blood circulation and biocompatibility of magnetic nanoparticles within the body.[27]

Developments of Fe_3O_4 nanoparticles for drug-carrying with diagnostic imaging not only require precision physical and chemical design, but also consider the pay of drug loading, transport, and release.[28-29] First, the coating type and loading way of Fe_3O_4 nanoparticles determine the abilities of carrying and protecting a significant drug payload. Second, Fe_3O_4 nanoparticles carefully loading with multiple drugs to accommodate the diverse therapeutics can overcome the cellular resistance, and increase the overall cell kill efficiencies. Third, the release mechanism and rate of the drug delivery system should be modulated for optimal therapeutic capability.[30] Since the large surface to volume ratio, Fe_3O_4 nanoparticles tend to agglomerate and absorb plasma proteins. To avoid these phenomena, coating with amphiphilic polymeric surfactants (poloxamers, poloxamines, and PEG) can stabilize nanoparticles and prolong the blood circulation time.[31] Moreover, modifying the targeting ligands increases the specific accumulation of nanoparticles within diseased tissue. By loading with different types of drugs, such as chemotherapeutic,[32-35] peptides and proteins,[36-38] DNA and siRNA,[39-44] Fe_3O_4 nanoparticles can apply to a wide range of diseases. For instance, Fe_3O_4 nanoparticles loading with chemotherapeutic agents, such as doxorubicin, etoposide, and methotrexate, have been used in breast and

prostate tumor therapy. Herceptin™, a protein, has been conjugated to magnetic nanoparticles as a mAb targeting molecule, which exhibits a therapeutic effect by causing cells to steady in G_1 phase of the cell cycle and thereby reduces cell proliferation. Fe_3O_4 nanoparticles conjugated with antisense oligodioxynucleotides for gene therapy significantly increase the half-time *in vivo*. Figure 2.8 shows the blueprint of multifunctional imaging/therapeutic magnetic nanoparticles and the local activity of several classes of drugs for cancer therapy.

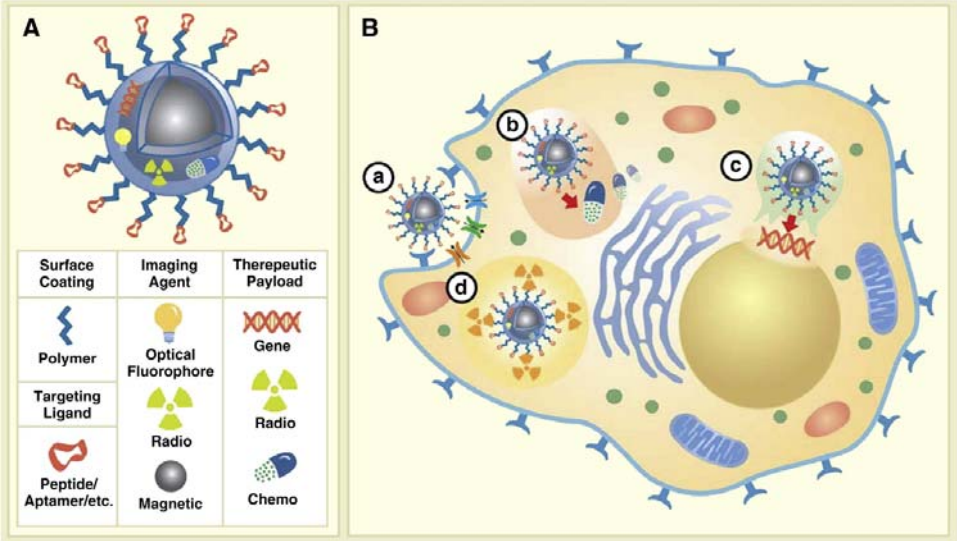

Figure 2.8 Illustration of multifunctional imaging/therapeutic MNPs anatomy and potential mechanisms of action at the cellular level. (A) A multifunctional MNP modified with targeting ligands extended from MNP surface with polymeric extenders, imaging reporters (optical, radio, magnetic), and potential therapeutic payloads (gene, radio, chemo). (B) Four possible modes of action for various therapeutic agents; a) Specific MNP binding to cell surface receptors (i.e. enzymes/proteins) facilitate their internalization and/or inactivation, b) controlled intercellular release of chemotherapeutics; c) release of gene therapeutic materials post endosomal escape and subsequent targeting of nucleus; and d) intracellular decay of radioactive materials.[30]

2.1.3 Hyperthermia

Although Fe_3O_4 nanoparticles don't carry any drugs, they still have therapeutic effects by themselves. Under high frequency magnetic field, Fe_3O_4 nanoparticles can generate heat energy due to the spin vibration by themselves, which is called hyperthermia. Since tumors are more sensitive to a temperature increase than healthy ones, the hyperthermia of Fe_3O_4 nanoparticles can be utilized to increase the temperature of tumor cells and thereby destroy the pathological cells.[45-46] The application of hyperthermia was first envisaged by Jordan et al. in 1993.[47] The amount of heat generated determines by the properties of magnetic nanoparticles and magnetic field parameters. For example, Marcela et al. have demonstrated that the heating rate of Fe_3O_4 nanoparticles are dependent on particle size at the same frequency magnetic field (Table 2.2).[48]

The main parameter determining the temperature increasing of the ferrofluid sample is the specific loss power (SLP), which is defined as the thermal power dissipation divided by the mass of magnetic nanoparticles and can be written as

$$\mathrm{SLP} = \frac{CV_s}{m}\frac{\mathrm{d}T}{\mathrm{d}t}$$

where C is the specific heat capacity of the sample, V_s is the sample volume, m is the mass of magnetic nanoparticles in the sample.

Sample	D_{TEM} (nm)	$D_{Chantrell}$ (nm)	σ	Concentration (m%)	χ_0	$SLP_{24.5\,kA/m}$ (W/g)
1	5	4.6	0.075	0.202	0.93	180
2	10	8.5	0.15	0.283	4.96	130
3	14	11.2	0.21	0.0867	12.31	447
4	12.8	9.6	0.22	0.252	7.98	200

Table 2.2 Size-dependent heating rates of iron oxide nanoparticles for magnetic fluid hyperthermia. Diameter measured with TEM, Chantrell method, polydispersity determined from Chantrell method, concentrations during calorimetry measurement, initial susceptibility and SLP measured at H_0=24.5 kA/m for ferrofluid amples.[48]

The heating effects of magnetic nanoparticles under a high frequency field are due to several types of loss processes, like hysteresis losses, Néel and Brown relaxation (Figure 2.9), the relative contributions of which depend strongly on the particle size. Magnetic nanoparticles with a diameter less than 30 nm are single-domain particles. Accordingly, their heat effects are governed by the combination of the rotational internal (Néel) and external (Brown) diffusion of particle magnetic moment.[49] Néel relaxation is due to thermal rotation of particle's magnetic moment within the crystal, which takes place when the anisotropy energy barrier (E_a=KV, where K the is anisotropy of the magnetic nanoparticles, V is the magnetic nanoparticls volume) is overcome. The characteristic time τ_N for Néel relaxation is expressed as $\tau_N=\tau_0 \exp(Ea/KV)$, where τ_0 is of the order of 10^{-9} s. Brown relaxation refers to thermal orientational fluctuations of the particle itself in the carrier fluid, the magnetic moment being locked onto the crystal anisotropy axis. The characteristic time τ_B for Brown relaxation is expressed as $\tau_B=3\eta V_H/kT$, where η is the viscosity of the carrier fluid, V_H is the hydrodynamic volume of the particle, k is the Boltzmann constant, T is the temperature. When the two relaxation mechanisms occur in parallel, the effective relaxation time τ is given by the relationship: $1/\tau=1/\tau_N+1/\tau_B$. Note that the shorter time determines the dominant mechanism of relaxation.[50]

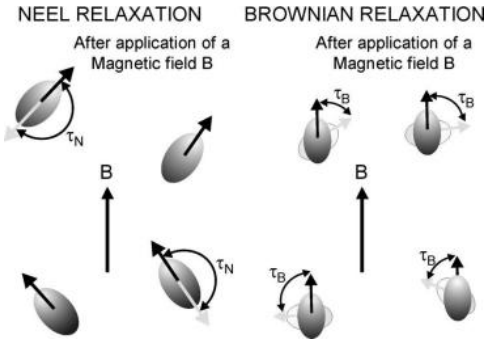

Figure 2.9 Illustration of the two components of the magnetic relaxation of a magnetic fluid.[51]

2.2 Core-Shell Nanoparticles

A core-shell nanoparticle is broadly defined as core and shell of different materials in close interaction, including inorganic, organic, biological core-shell combination. There are numerous advantages make core-shell nanoparticle playing an important role in material chemistry, including (1) size monodispersity, (2) core and shell processibility, (3) stability, (4) solubility, (5) tunability, (6) self-assembling capability, (7) reactivities involving in chemical, biological, magnetic, optical, electric, and catalytic phenomena. Consequently, core-shell nanoparticles have a variety of application range from magnetic, quantum dots, microelectronic, and photoactive devices.

Following are some examples of various types of core-shell nanoparticles. The monodispersed CdSe nanocrystals coating with a ZnSe shell show high room temperature photoluminescence efficiencies (60-85%) in organic solvents as well as in water after modification with mercaptoundecanoic acid (MUA) (Figure 2.10).[52]

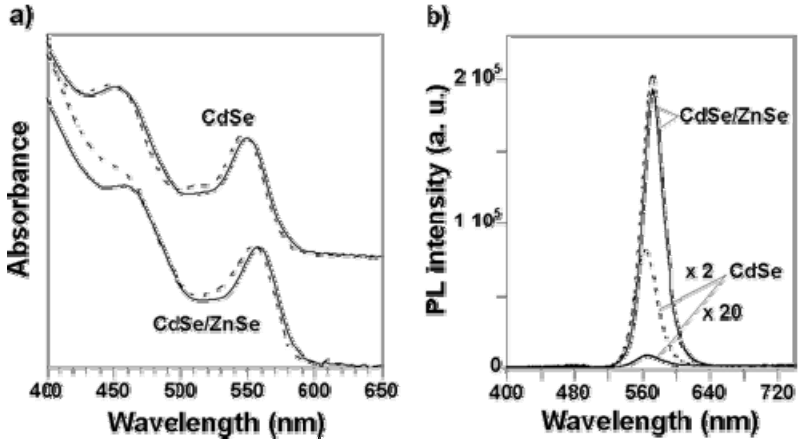

Figure 2.10 Absorption (a) and photoluminescence (b) spectra of CdSe core and CdSe/ZnSe core/shell nanocrystals before (dashed lines, toluene solutions) and after (solid lines, aqueous solutions) functionalization with MUA. All colloidal solutions exhibit identical optical densities at the first exciton absorption peak.[52]

An Ag core with Au shell nanoparticle, which exhibits a Surface Plasmon band between 390 nm and 420 nm with larger extinction coefficient of sliver but the stability and surface chemistry of gold, has been used to access a colorimetric detection system distinct from a pure gold system (Figure 2.11).[53] The luminescent and magnetic nanoparticles, which were easily separated from solution by magnetic decantation using a permanent magnet, have been synthesized by coating CdSe/ZnS shell on γ-Fe_2O_3 superparamagnetic core (Figure 2.12).[54] Due to the various properties of each materials, someone can synthesize a novel material for their own use by combining different materials into a core-shell nanoparticle.

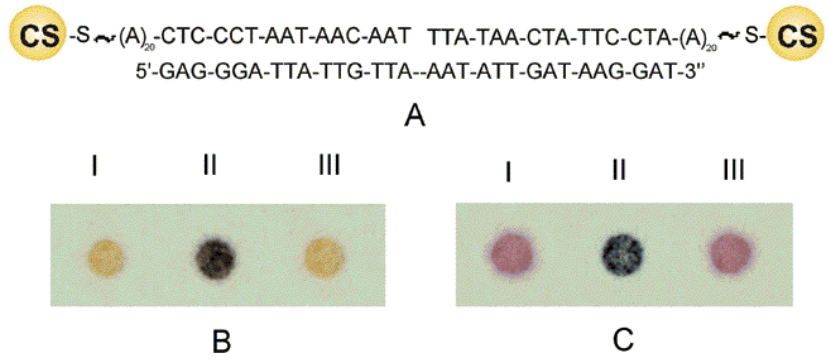

Figure 2.11 (A) Mercaptoalkyl-oligonuleotide-modified Ag core/Au shell particles and polynucleotide target. DNA spot test using: (B) 12.4 nm Ag/Au nanoparticle probes and (C) 13 nm Au nanoparticle probes: (I) without target, (II) with target at room temperature, (III) with target at 58.0°C, a temperature above the T_m (53.0°C) of the hybridized DNA.[53]

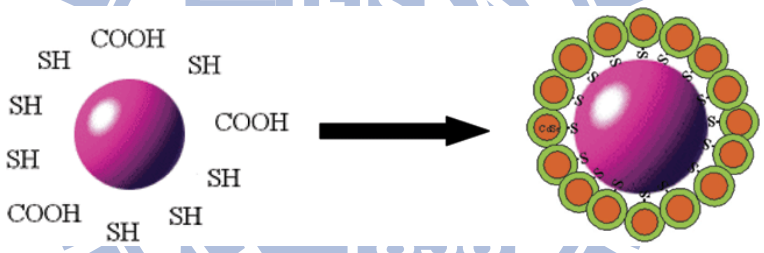

Figure 2.12 Thiol and carboxy modified γ-Fe_2O_3 beads are reacted with CdSe/ZnS QDs to form the luminescent/magnetic nanocomposite particles.[54]

2.3 Doxorubicin

Cancer, one of the most terrible diseases, is caused by DNA mutation, rearrangement, and deletion, which introduce oncogenes to promote cell irregularly growth and reproduction. Thus, developing of anticancer drugs are usually focusing on the interaction with DNA molecules, such as DNA alkylation agent, intercalating agent, cleaving agent, and binding agent. After interacting with DNA molecules, the anticancer drugs affect the DNA replication, transcription, and translation.

Doxorubicin (Figure 2.13) is one of anthracyclin antibiotics, which are the most powerful weapons in the chemical arsenal used for cancer chemotherapy. The binding mechanisms contain (1) the planar anthraquinone ring system intercalating into DNA, (2) the puckered anchor D ring giving additional contacts to DNA via direct and indirect hydrogen-bonding interactions, and (3) the daunosamine sugar playing a role in a minor groove binder and recognition of the DNA base surface within the helical groove.[56] When doxorubicin binding with DNA, it will stabilize the topoisomerase Ⅱ complex, keeping the DNA double helix from separating and thereby stopping the process of replication.

Doxorubicin has been commonly used in the treatments of a wide range of cancers, including breast cancer, lung cancer, hematological malignancies, and soft tissue sarcomas. The normal dosage is 20 mg/m^2 every week or 60-75 mg/m^2 every 3 weeks.[57] However, high accumulative doses of doxorubicin increase the probability of cardiotoxicity (e.g. 550 mg/m^2 of accumulative doxorubicin has 7% probability of cardiotoxicity).[58] Therefore, exploring a escort of delivery molecule to reduce the side effects is necessary.

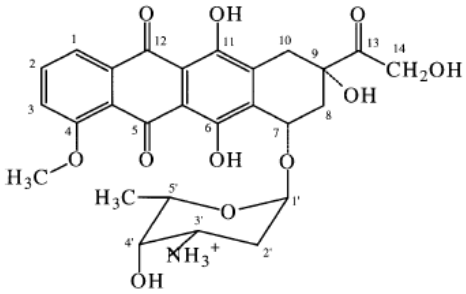

Figure 2.13 Structure of doxorubicin.[55]

2.4 Motivation

Cancer has threatened the lives of humankind for many years. Despite the fact that the cure for cancer had taken effect in recent years, repeated diagnosis (e.g. magnetic resonance imaging, ultrasound, computed tomography, and positron emission tomography) and treatments (e.g. surgery, chemotherapy, and radiation therapy) have been bringing infinite sufferings to the patients instead of pains caused by cancer itself. Therefore, developing a multifunctional pharmaceutical that can simultaneously perform various functions, including targeting, imaging, and therapy, is necessary.

As we all know, nanomaterials, such as quantum dots, superparamagnetic iron oxide nanoparticles, and gold nanoparticles, have been investigated for potential multifunctional purposes as imaging agents capable of visualization by MR imaging or optical imaging techniques, therapeutic agents, and delivery vehicles. In the various nanomaterials, superparamagnetic nanoparticles become more and more popular owing to their potential in MR imaging which plays an important role in non-invasive imaging. In addition, the magnetic property of magnetic nanoparticles make themselves can be heated by high frequency magnetic fields and manipulated by an external magnetic field. Thus, magnetic nanoparticles have been extensively used in biomedical applications. Fe_3O_4 nanoparticle is one of the magnetic nanoparticles which can be simply synthesized under atmosphere at room temperature by co-precipitation. However, particles prepared by co-precipitation tend to be polydispersed. In order to improve this phenomenon, introducing a gold shell around them makes they more stable and highly monodispersed. In addition, gold surface is in favor of functionalization with thiolated biomolecules.

By modifying double strand DNA, which are thermo-sensitive molecules and can be denatured of the double helix to form two single strands, the anticancer drug,

doxorubicin, can be carried by intercalation. When high frequency magnetic field heated the superparamagnetic nanoparticles, the modified double strand DNA would unwind and release the anticancer drugs. By adjusting duration time under high frequency magnetic field, the drug delivery can be tuned. Therefore, a multifunctional system including imaging, targeting, and tunable drug delivery could be integrated into a Fe_3O_4 core/Au shell nanoparticle (Figure 2.14).

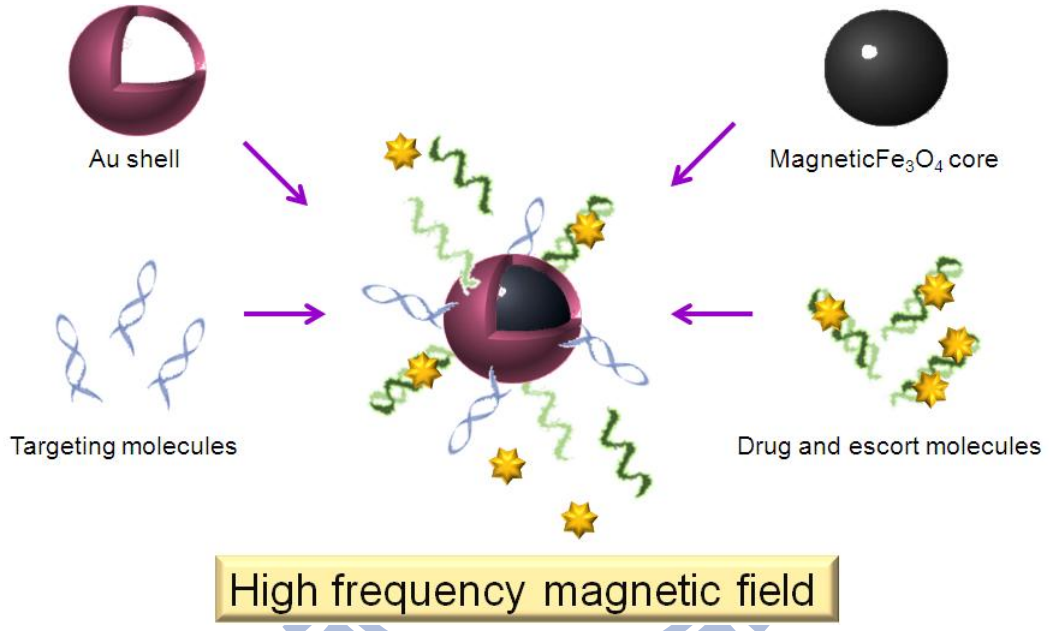

Figure 2.14 A multifunctional system including imaging, targeting, and tunable drug delivery could be integrated into a Fe_3O_4 core/Au shell nanoparticle.

Chapter 3: Experiments

3.1 General Introduction

All the experiments were preceded in National Chiao Tung University (NCTU). All the equipments were also conducted in our laboratories in NCTU. The reagents were purchased commercially and used by following with the directions unless specially mentioned.

All the reagents were listed alphabetically in the form of "Name {abbreviation; chemical formula; purity; manufacturer}". Some information will be omitted if not available or not necessary. The following text will use the abbreviation of the reagent.

Deionized and distilled water {DI water, ddH2O}

The water we used was purified with filters, reverse osmosis, and deionized system until the resistance was more than 18 MΩ • cm^{-1}. DI water was used to clean, wash, and be a solvent.

Iron(Ⅱ) chloride tetrahydrate {$FeCl_2 \cdot 4H_2O$, 98%; Alfa Aesar}

The chemical provided Fe^{2+} ion for the co-precipitation of Fe_3O_4 nanopaticles synthesis.

Iron(Ⅲ) chloride hexahydrate {$FeCl_3 \cdot 6H_2O$, 98%; Alfa Aesar}

The chemical provided Fe^{3+} ion for the co-precipitation of Fe_3O_4 nanopaticles synthesis.

Hydrogen chloride {HCl, ≥99% purity; Sigma}

It was used to dissolve iron(Ⅱ) chloride tetrahydrate and iron(Ⅲ) chloride hexahydrate for Fe_3O_4 nanopaticles synthesis.

Sodium hydroxide {NaOH, 97%; SHOWA}

This pellets was dissolved in DI water to yield 3 M sodium hydroxide solution, which provided the alkaline environment to prepared Fe_3O_4 nanopaticles by co-precipitation of Fe(Ⅱ) and Fe(Ⅲ) chlorides in an alkaline solution.

Tetramethylammonium hydroxide {$(CH_3)_4NOH$, 25% w/w in aqueous solution; Fluka }

This alkaline solution was diluted with DI water for various concentrations to improve the dispersion of Fe_3O_4 nanoparticles.

Gold(Ⅲ) chloride trihydrate {$HAuCl_4 \cdot 3H_2O$, ≥49%; Sigma}

The chemical was a provider of Au^{3+} ion for the mechanism of Au nanoshell synthesis.

Trisodium citrate dihydrate {$C_6H_5Na_3O_7 \cdot 2H_2O$, 98%; SHOWA}

We used a previously reported chemical reduction method to prepare Au nanoshell in aqueous solution. This chemical was a reductant of the reaction. Prior to use, the powder needed to dissolve in the DI water.

Hydroxylamine hydrochloride {$NH_2OH \cdot HCl$, 99%; Alfa Aesar}

The powder was dissolved in the DI water, and was used in the reaction of coating Au nanoshell onto the Fe_3O_4 nanopaticles.

Drug delivery oligonucleotides

A short nucleic acid polymer, typically has fifty or fewer bases. In this study, oligonucleotides were obtained from MDBio, Inc. (Taiwan) and hybridized to form double strand DNA for drug carrying. The DNA sequences were showed in Table 3.1.

Name	Sequence
T3	5'-CGA CGA CGA CGA CGA CGA TTT-3'
A15	SH-5'-AAA AAA AAA AAA AAA TCG TCG TCG TCG TCG TCG-3'
A15T3	5'-CGA CGA CGA CGA CGA CGA TTT-3' 3'-GCT GCT GCT GCT GCT GCT AAA AAA AAA AAA AAA-5'-SH

Table 3.1 The DNA sequences.

Doxorubicin hydrochloride {$C_{27}H_{29}NO_{11}$·HCl, ≥98%; Sigma}

This molecule played roles as both anticancer drug and fluorescence agent, which had an exciting wavelength at 470 nm and an emission wavelength at 590 nm.

3.2 Assaying the Specimen

(A) SEM

SEM is a very useful tool for observing surface morphology of specimen. SEM has secondary electrons or backscattered electrons detectors passing the signal to computer and forming image. In this study, the morphology and microstructure of the Fe_3O_4 nanoparticles and Fe_3O_4 core/Au shell nanoparticles were all characterized by a field-emission SEM (FE-SEM) (JEOL-6700) operating at 10 kV accelerating voltage.

(B) XRD

X-ray powder diffraction (XRD) is a rapid analytical technique primarily used for the study of crystal structures and atomic spacing. X-ray diffraction is based on constructive interference of monochromatic X-rays and a crystalline sample. It can show the phase identification of a crystalline material and can provide information on unit cell dimensions. The analyzed material is finely ground, homogenized, and average bulk composition is determined. The interaction of the incident rays with the sample produces constructive interference (and a diffracted ray) when conditions satisfy Bragg's Law ($n\lambda=2d$ sin θ). These diffracted X-rays are then detected, processed and counted. By scanning the sample through a range of 2θ angles, all possible diffraction directions of the lattice should be attained due to the random orientation of the powdered material and then to converse the diffraction peaks to d-spacings allows identification of the mineral because each mineral has a set of unique d-spacings. In this study, the microstructure of the Fe_3O_4 nanoparticles and Fe_3O_4 core/Au shell nanoparticles were all characterized by an aid of x-ray diffraction (X'Pert PRO MRD system).[59]

(C) TEM

Transmission electron microscopy (TEM) is a microscopy technique. By shooting an electronic beam to transmit an ultra thin specimen, it can observe the internal morphology and crystal atomic structure of specimen. In this study, TEM (JEOL, JEM-2010) was used to examine the internal morphology and electron diffraction of the Fe_3O_4 nanoparticles and Fe_3O_4 core/Au shell nanoparticles.

(D) EDS

Energy dispersive X-ray spectroscopy (EDS) is an analytical technique used for the elemental analysis or chemical characterization of a sample. It relies on the investigation of a sample through interactions between electromagnetic radiation and matter, analyzing x-rays emitted by the matter in response to being hit with charged particles. Its characterization capabilities are due in large part to the fundamental principle that each element has a unique atomic structure allowing x-rays that are characteristic of an element's atomic structure to be identified uniquely from each other.[60] In our experiment, EDX (Oxford-Link ISIS 300 energy-dispersive X-ray) give our analytical of elements for the specimen under TEM monitoring.

(E) SQUID

Superconducting quantum interference device (SQUID, MPMS-XL) is an ultra sensitive magnetometer used to measure extremely subtle magnetic field of Fe_3O_4 nanoparticles and Fe_3O_4 core/Au shell nanoparticles, which based on superconducting loops containing Josephson junctions.

(F) Delsa^{TM} Nano Submicron Particle Size and Zeta Potential

Zeta potential is a scientific term for electronkinetic. The value of zeta potential, which can be related to the stability, is the potential difference between the dispersion medium and the stationary layer of fluid attached to the dispersed particle. The zeta potential of Fe_3O_4 nanoparticles and Fe_3O_4 core/Au shell nanoparticles is measured by Delsa^{TM} Nano Submicron Particle Size and Zeta Potential (BECKMAN COULTER, PN A54412AA) in this study.

(G) UV-Vis Spectroscopy

UV-Vis spectroscopy uses light in the range of near UV, visible and near infrared. The absorption in the light range is due to the optical properties of the chemicals involved. We determine whether the Fe_3O_4 nanoparticles covered by Au shell or not in the visible range of 400-800 nm by the UV-Vis spectroscopy (HITACHI, U-3310).

(H) Fluorescence Spectroscopy

Fluorescence spectroscopy (HITACHI, F-7000) is used to measure the doxorubicin release from Fe_3O_4 core/gold shell nanoparticle carrier by shooting a 470 nm light to excite the electrons in doxorubicin molecule and measuring the intensity of 590 nm light emitting from the exciting electrons to determine the concentration of doxorubicin.

(G) HFMF

High frequency magnetic field is a machine which can provide oscillating magnetic field to heat the magnetic materials. In this study, high frequency magnetic field (GE-15) with a frequency of 50 kHz and a magnetic field strength (H) of 8 kA/m was used to heat Fe_3O_4 nanoparticles and Fe_3O_4 core/Au shell nanoparticles due to Néel and Brown relaxation of superparamagnetic nanoparticles in oscillating magnetic field.

3.3 Experimental Methods

The synthetic flow includes synthesis of Fe_3O_4 nanoparticles, coating Au shell onto Fe_3O_4 nanoparticles, DNA hybridization, modifying with double strand DNA, intercalating doxorubicin, and drug release test (Figure 3.1).

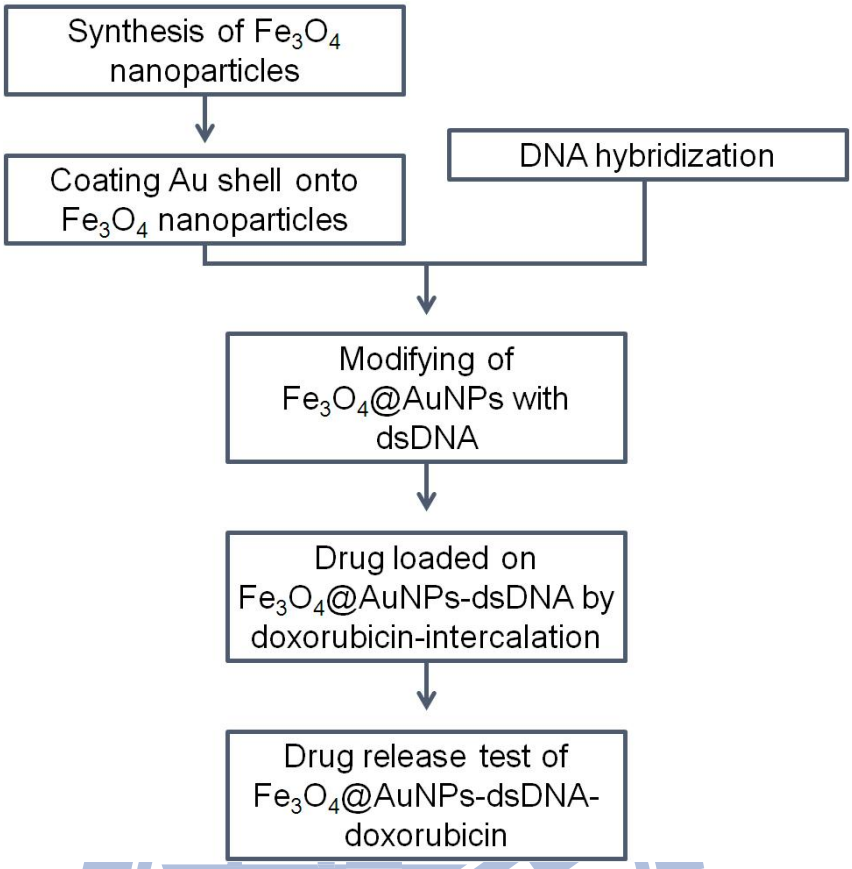

Figure 3.1 The experimental flowchart.

3.3.1 Preparation of Fe_3O_4 Nanoparticles

The Fe_3O_4 nanoparticles were prepared in aqueous solution using a previously reported co-precipitation method.[17] Firstly, 0.4 g of $FeCl_2 \cdot 4H_2O$, 1.04 g of $FeCl_3 \cdot 6H_2O$ and 170 μl 12 M HCl were dissolved in 5 mL of DI water for 30 min with stirring. Secondly, the solution was added dropwise into 25 mL of 3 M NaOH solution with vigorous stirring, and then a black precipitate formed immediately. Finally, the precipitate was isolated by a mighty magnet, and washed twice with DI water, and then resuspended in 0.1 M $(CH_3)_4NOH$ solution. The black, 6.5 mg/mL magnetic nanoparticle solution was stored in air under benchtop conditions for further use.

3.3.2 Preparation of Fe_3O_4@Au Nanoparticles

Fe_3O_4 core/Au shell nanoapeticles were synthesized by deposition of Au on the performed Fe_3O_4 nanoaprticles using a modification of Lyon's iterative hydroxylamine seeding procedure.[61] First, 1 mL of Fe_3O_4 nanoparticles solution was stirred with 1 mL of 0.1 M sodium citrate for 10 min. Next, the solution was diluted with DI water to 20 mL, and 100 μL of 80 mM $NH_2OH{\cdot}HCl$ solution was added. Then 2 mL of 1% $HAuCl_4$ solution was added dropwise with stirring. Finally, the uncoated Fe_3O_4 nanoparticles were removed by centrifugation.

3.3.3 DNA Hybridization

The boughten oligonucleotides, which look like white powder, were dissolved in TE buffer (10 mM Tris-HCl/1 mM EDTA)/50 mM NaCl with pipetting to form ssDNA solution. A15T3 dsDNA was hybridized by mixing A15 ssDNA and T3 ssDNA sequences at a 1: 1 molar ratio, heating the solution to 95°C for 10 min in a large water bath, and then cooling slowly to room temperature. The obtained dsDNA was stored in 4°C.

3.3.4 Fe_3O_4@AuNPs-Bound dsDNA

For preparation of drug carrier, the dsDNA were added into Fe_3O_4@AuNP solution. The drug carrier was made by mixing 1 mL of 0.1mg/mL Fe_3O_4@AuNP solution and 10 μL of 50 mM dsDNA for 6 h at room temperature. To remove unbound dsDNA, the solution was centrifuged, and the pellet was washed with DI water twice, and then resuspended in 1 mL of DI water (Figure 3.2).

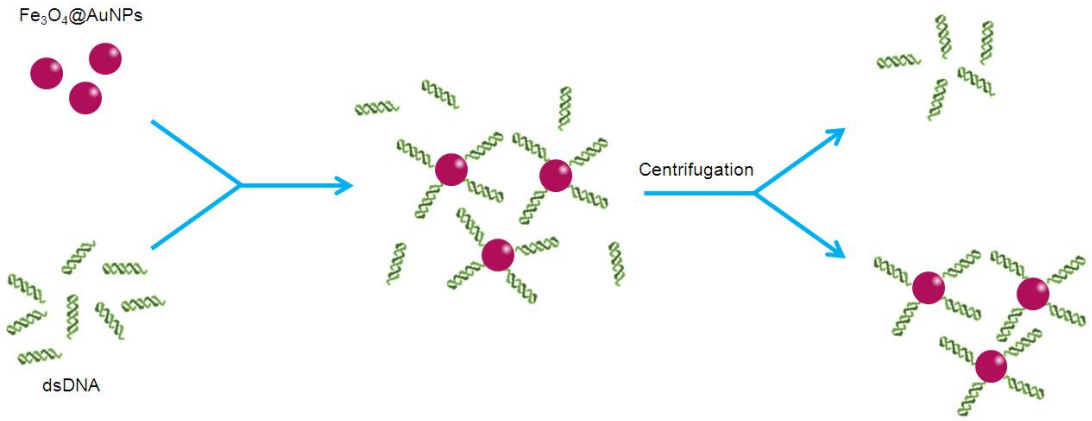

Figure 3.2 Schematic steps for the preparation of Fe_3O_4@AuNPs-bound dsDNA.

3.3.5 Doxorubicin-Intercalated Fe_3O_4@AuNPs-dsDNA

For drug loading, 1 mL of 0.1mg/mL Fe_3O_4@AuNP-dsDNA was mixing with 5μL of 1.72 mM doxorubicin for 3 h at room temperature. The unintercalated doxocrubicin were removed by centrifugation, and the pellet was resuspended in 1 mL of DI water (Figure 3.3).

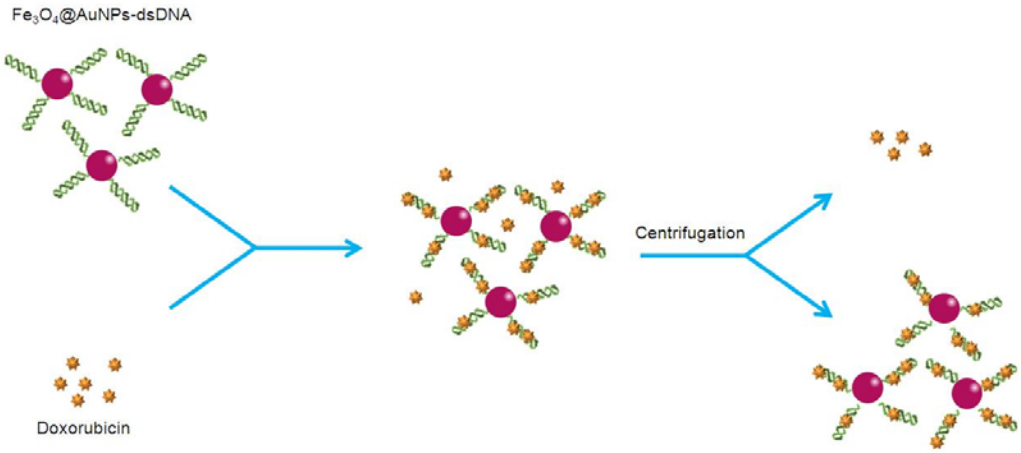

Figure 3.3 Schematic steps for the preparation of doxorubicin-intercalated Fe_3O_4@AuNPs-dsDNA.

3.3.6 Drug Delivery of Fe_3O_4@AuNPs-dsDNA-Doxorbuicin at Various Temperatures

For testing the drug release as a function of temperature, each 1 mL of Fe_3O_4@AuNP-dsDNA-doxocrubicin was put into water bath with different temperature for 10 min, and then the sample was immediately removed and centrifuged to collect the supernatant, which contained the released doxorubicin. To determine the release rate, the fluorescence intensity of the supernatant was measured.

3.3.7 Drug Delivery of Fe_3O_4@AuNPs-dsDNA-Doxorbuicin under High Frequency Magnetic Field

For inducing drug release by high frequency magnetic fields, 1 mL of Fe_3O_4@AuNP-dsDNA-doxocrubicin was put in the center of the loop of high frequency magnetic field without any contact for different time periods (Figure 3.4). After treating with high frequency magnetic field, the sample was immediately removed and centrifuged to collect the supernatant, which contained the released doxorubicin. By measuring the fluorescence intensity of the supernatant, the release rate induced by high frequency magnetic field was determined.

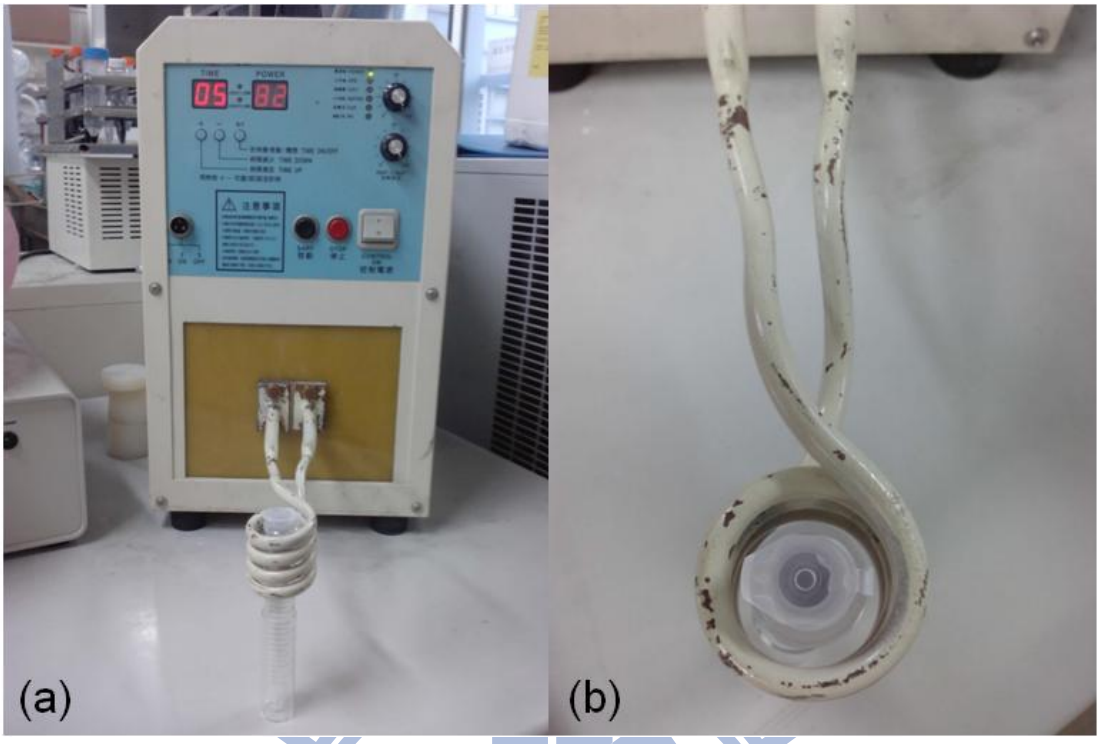

Figure 3.4 (a) Equipment of drug release induced by high frequency magnetic field. (b) The sample was put in the center of the loop without any contact.

Chapter 4: Results and Discussion

4.1 Synthesis and Characterization of Fe_3O_4 Nanoparticles and Fe_3O_4@Au Nanoparticles

This section describes the results of Fe_3O_4 nanoparticles and Fe_3O_4@Au nanoparticles with SEM, TEM, EDS, XRD, SAED, zeta-potential, and magnetic properties analysis.

4.1.1 Synthesis of Fe_3O_4 Nanoparticles and Fe_3O_4@Au Nanoparticles

At first step, we synthesized Fe_3O_4 naniparticles by co-precipitation. The particles showed a black color, and can be isolated by a magnet (Figure 4.1). Although the newly synthesized particles presented a serious aggregation, which were common in co-precipitation,[16] 0.01 M tetramethylammonium hydroxide (TMAOH) was introduced to the solution for improving this phenomenon. Dramatically, the particles showed more dispersed. By increasing the concentration of TMAOH from 0.01 M to 0.1 M, the particles exhibited a more monodispersed morphology. Further, dispersing the particles in 0.1 M TMAOH with sonication, the isolated Fe_3O_4 nanoparticles were appeared (Figure 4.2). The improvement may be contributed to the existence of TMAOH, which is a strong alkaline. The effect of TMAOH will discuss in 4.1.2. With monodispersed morphology, Fe_3O_4 nanoparticles had good performances in MR imaging for medical diagnosis, controlled drug delivery, biological targeting, and catalysis.

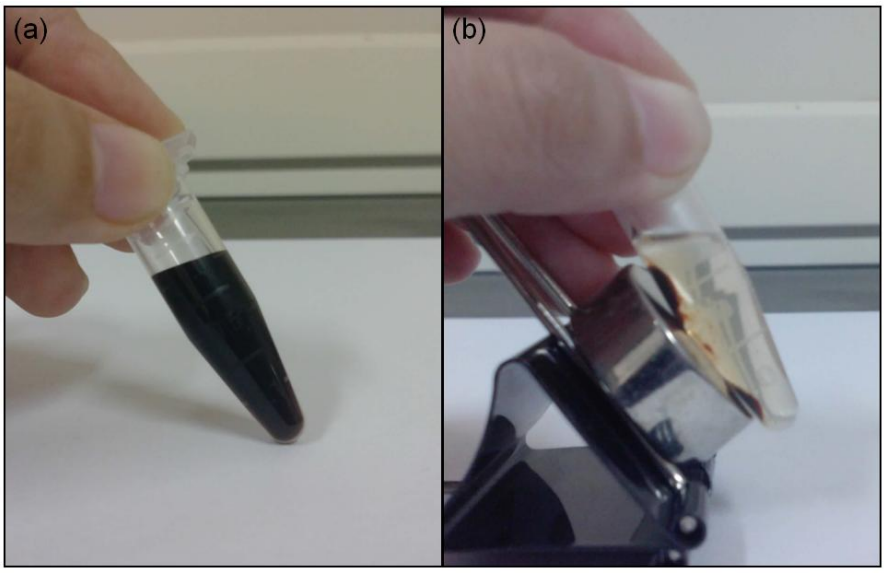

Figure 4.1 (a) Fe_3O_4 nanoparticles synthesized by co-precipitation showed a black color, and (b) were concentrated by a magnet.

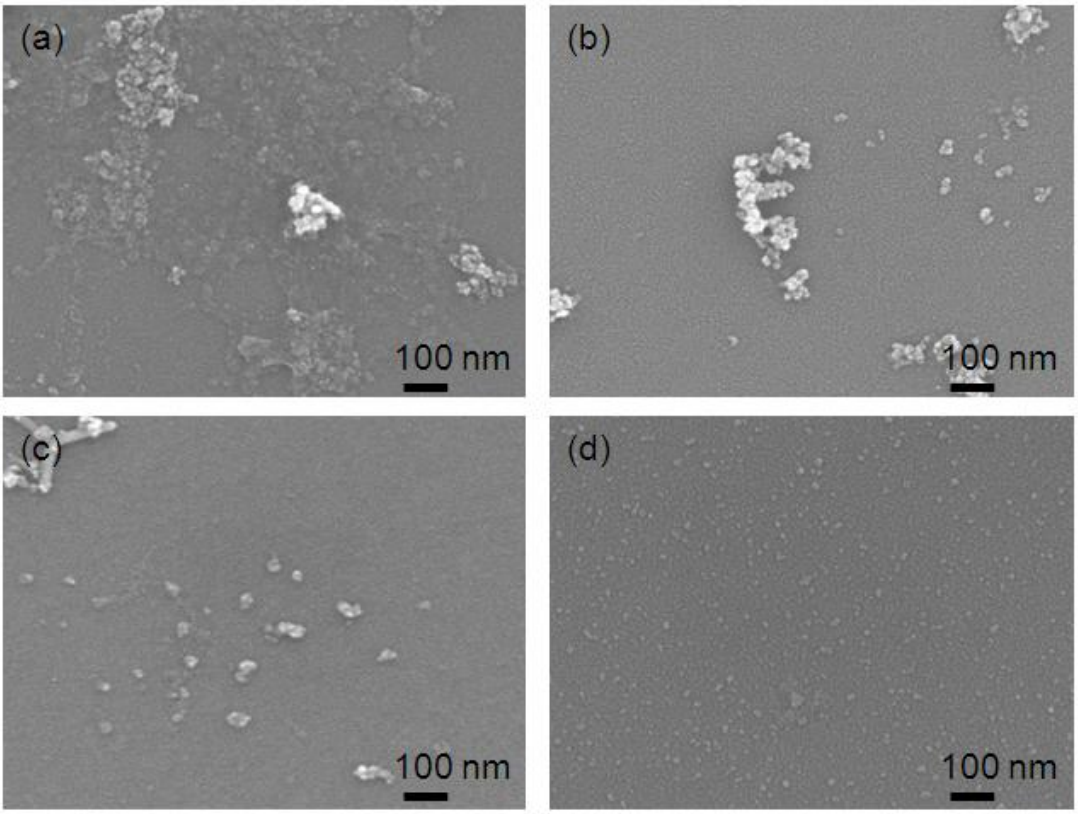

Figure 4.2 SEM images of Fe_3O_4 nanoparticles in different solvents: (a) DI water, (b) 0.01 M TMAOH, (c) 0.1 M TMAOH, (d) 0.1 M TMAOH with sonication.

Since Fe_3O_4 nanoparticles, which had a large ratio of surface-area to volume, tend to agglomerate in order to reduce their surface energy by strong magnetic dipole-dipole attractions between particles. Au shell was covered to enhance chemical stability for protecting the magnetic core from oxidation and corrosion, as well as exhibit good biocompatibility and affinity via thiol/amine terminal groups.

After the process of coating Au shell, the particles which can still be isolated by a magnet, exhibited a pink color (Figure 4.3), with the particle size about 40 nm. The UV-Vis spectrum also showed a strong Surface Plasmon Resonance (SPR) at ca. 530 nm, which was not shown on the Fe_3O_4 nanoparticles (Figure 4.4). Among pure Au nanoparticles, the collective oscillations of free electrons, known as Surface Plasmon (SP), cause an absorption peak to appear in the visible region of the electromagnetic spectrum.[62] Factors that affect the position of the SP peak have been investigated on the basis of Mie theory; for Au nanoparticles, the SP has been shown to shift as a function of particle size, and stabilizing ligand.[63-68] Therefore, the bimetallic core/shell nanoparticles were further characterized by UV-Vis spectroscopy to compare the optical properties to those of pure Au nanoparticles.[61] Au nanoparticles, which exhibit a 530 nm absorption, have corresponsive 48 nm particle size.[69] However, the particles prepared in this work exhibited 530 nm absorption with the size of 40 nm. This phenomenon could result from the charge variation of the Au particles within the core/shell structure.[70]

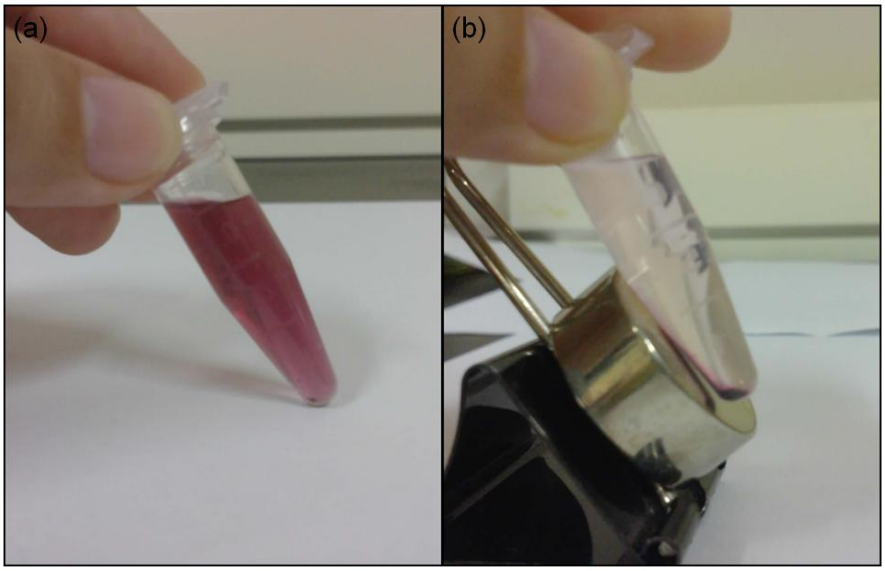

Figure 4.3 (a) Au shell processed Fe_3O_4 nanoparticles showed a pink color, and (b) were concentrated by a magnet.

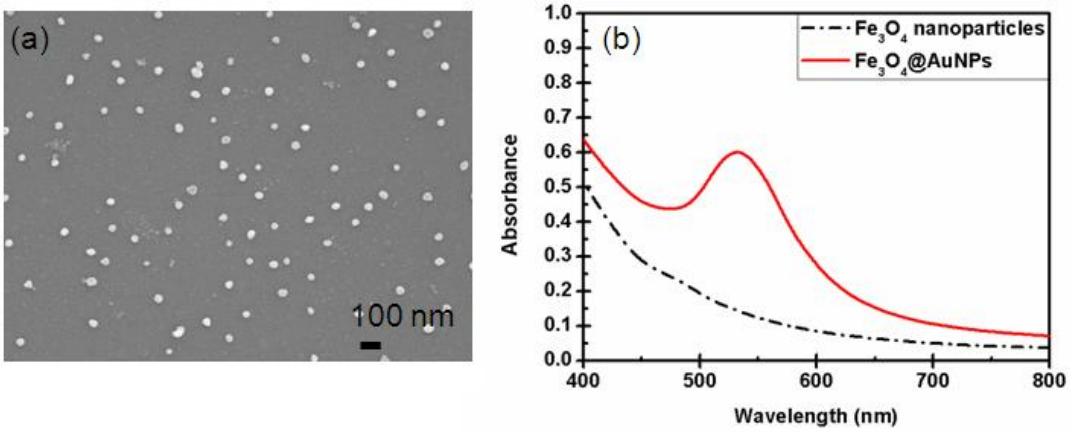

Figure 4.4 (a) SEM image of the Fe_3O_4 nanoparticles after coating Au shell. (b) UV-Vis spectrum of Fe_3O_4 nanoparticles (dash) and Fe_3O_4 nanoparticles after coating Au shell (solid).

4.1.2 Zeta-potential of Fe_3O_4 Nanoparticles and Fe_3O_4@Au Nanoparticles

Zeta-potential is a value typically for quantifying the charge distribution, which represents the coupled effect of the conjugate's charge and the ionic conditions of the

solution. Thus, the changes of particle surface due to the addition of different surfactants can be figured out by zeta-potential measurement. As shown in Table 4.1, the zeta-potential of Fe_3O_4 nanoparticles in DI water, 0.01 M TMAOH, and 0.1 M TMAOH were -38.84 mV, -40.84 mV, and -43.61 mV respectively; it was showed that the most negative value of Fe_3O_4 nanoparticles in 0.1 M TMAOH. It is well known that TMAOH is a strong alkaline, which can make the surface of the Fe_3O_4 nanoparticles more negative charged in stronger alkaline medium. Therefore, with increased amount of TMAOH, zeta-potential of the nanoparticles becomes more negative.[71] Further, after coating Au shell, the zeta-potential value increasing to -52.7 mV, showed the most negative charge of Fe_3O_4@Au nanoparticles.

Sample	Zeta-potential
Fe_3O_4 nanoparticles in DI water	-38.84 mV
Fe_3O_4 nanoparticles in 0.01 M TMAOH	-40.84 mV
Fe_3O_4 nanoparticles in 0.1 M TMAOH	-43.61 mV
Fe_3O_4@Au nanoparticles	-52.7 mV

Table 4.1 Zeta-potential of Fe_3O_4 nanoparticles in DI water, 0.01 M TMAOH, 0.1 M THAOH, and Fe_3O_4@Au nanoparticles.

4.1.3 Size Distribution of Fe_3O_4 Nanoparticles and Fe_3O_4@Au Nanoparticles

With the Au shell we have capped, the difference of particle size between Fe_3O_4 and Fe_3O_4@Au could be an evidence for existence of Au shell. For this purpose, the size distribution of Fe_3O_4 nanoparticles and Fe_3O_4@Au nanoparticles were measured.

The particle size of the Fe_3O_4 nanoparticles and the Fe_3O_4@Au nanoparticles were calculated by the software named Image-pro plus (IPP), and the analysis region were the full SEM images of Figure 4.2 (d) and Figure 4.3 (a). The average size of the Fe_3O_4 nanoparticles and the Fe_3O_4@Au nanoaprticles were 9.6±3 nm and 38.1±5.5 nm (Figure 4.5). In other words, the thickness of Au shell wrapped on Fe_3O_4 could be calculated as about 14.25 nm with narrow size distribution. Besides, particle size is of great importance in design of nanomaterials for targeted drug delivery. Particles larger than 150 nm could be removed rapidly by liver and spleen after injection, resulting in poor *in vivo* circulation time and targeting efficiency; while particles smaller than 20 nm have been reported to be excreted through renal clearance, which will also decrease the longevity of the particles after injection *in vivo*.[72-73] Thus, the particle size of Fe_3O_4@Au nanoparticles prepared in this work fell into the suitable range.

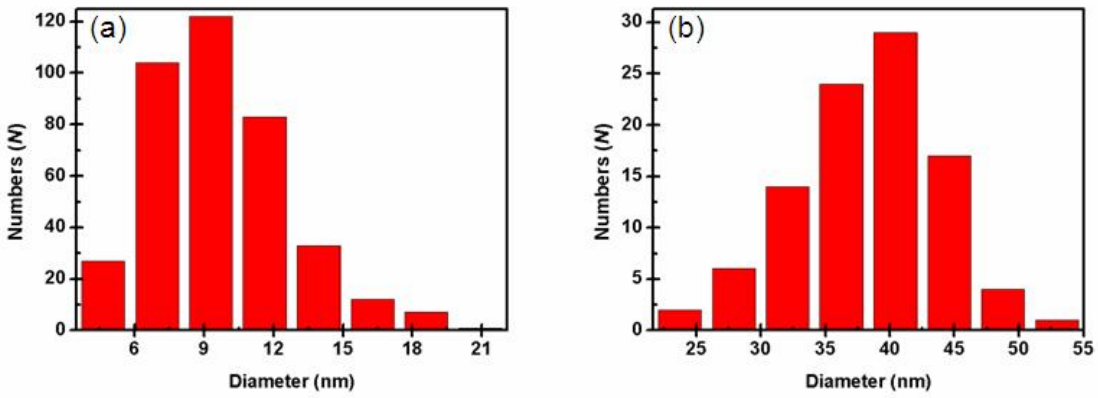

Figure 4.5 Size distributions of (a) Fe_3O_4 nanoparticles, (b) Fe_3O_4@Au nanoparticles.

4.1.4 Characterization of Fe_3O_4 Nanoparticles and Fe_3O_4@Au Nanoparticles

Although all the SEM images indicated the existence of Au shell, TEM images, EDS spectrum, XRD spectra, and SAED patterns were used to further investigate the compositions and structures of Fe_3O_4 nanoparticles and Fe_3O_4@Au nanoparticles.

From the TEM images (Figure 4.6), the color differences of outer and inner particles showed a core/shell morphology, and all the particles had a uniform size about 40 nm without any aggregation, which corresponded to SEM image. Furthermore, both the SEM and TEM images did not show any Fe_3O_4 nanoparticles, illustrating that centrifugation to remove uncoated Fe_3O_4 nanoparticles was effective. In addition, to confirm the composition of the particles, EDS spectrum were collected during TEM imaging. This spectrum (Figure 4.7) confirmed the presence of both Fe and Au elements in the Fe_3O_4@Au nanoparticles. Cu peaks were caused by scattering of the Cu TEM grid.

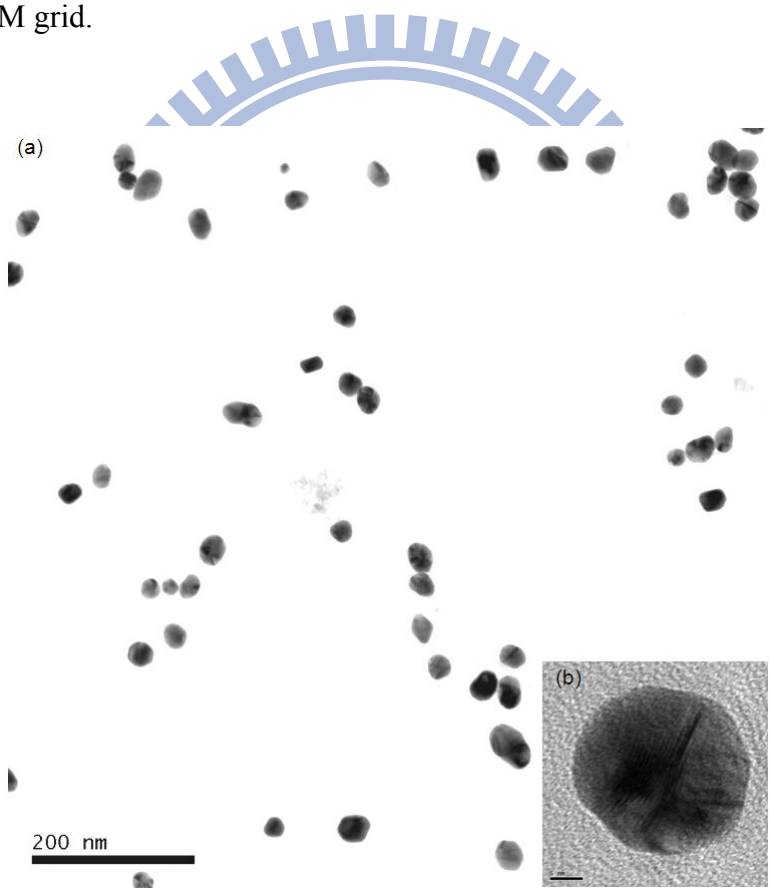

Figure 4.6 (a) TEM image of the Fe_3O_4 nanoparticles processed coating Au shell. (b) The particles exhibited core/shell morphology.

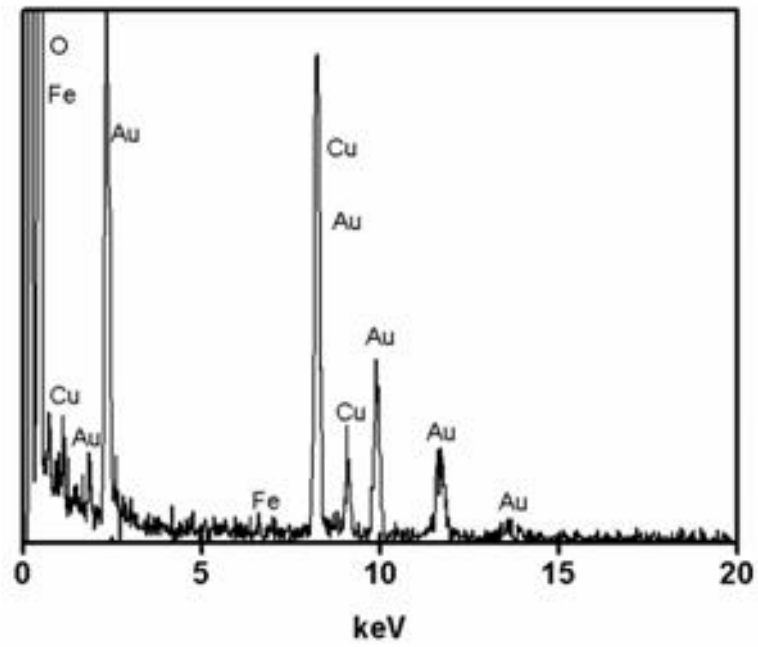

Figure 4.7 EDS spectrum of the sample used to obtain Figure 4.6.

XRD spectrum was used to verify crystal structure and atomic spacing by constructive interference of monochromatic X-rays and a crystalline sample. The XRD pattern of Fe_3O_4 nanoparticles showed diffraction peaks at 21.16°, 30.11°, 35.53°, 43.12°, and 62.61° which can be indexed to the (002), (112), (103), (004), and (224) plans of Fe_3O_4 in a cubic phase with the standard pattern of the Joint Committee of Power Diffraction Standard (JCPDS) code of 75-1609. The XRD pattern of Fe_3O_4@Au nanoparticles showed diffraction peaks at 38.18°, 44.38°, 64.57°, and 77.56° which can be indexed to the (111), (200), (220), and (311) plans of Au in a cubic phase with JCPDS code of 65-2870. The XRD data showed the peaks of Fe_3O_4@Au nanoparticles correspond to gold (Au) but magnetite phase (Fe_3O_4). This phenomenon may be contributed to the high ratio of Au to Fe_3O_4 (Figure 4.8). The results indicated that the prepared Fe_3O_4 nanoparticles can be confirmed as composition of Fe_3O_4, and the prepared Fe_3O_4@Au nanoparticles can prove the existence of Au.

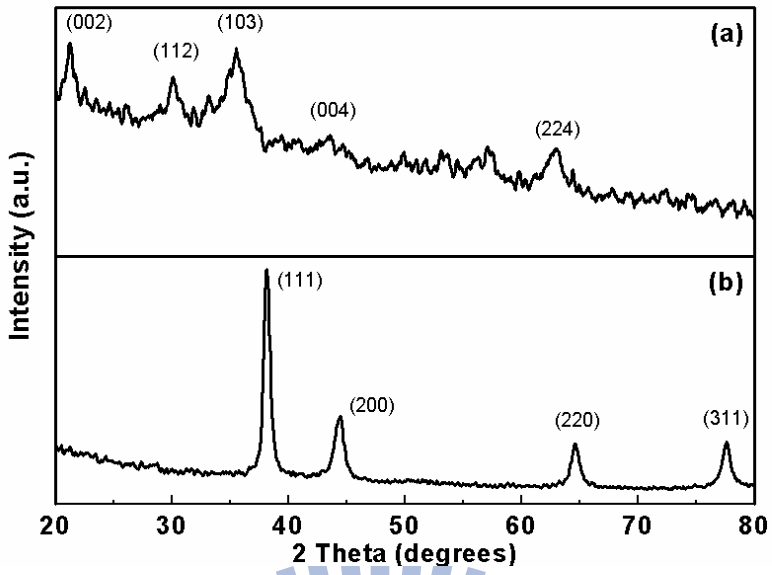

Figure 4.8 XRD spectra of (a) Fe_3O_4 nanoparticles, and (b) Fe_3O_4@Au nanoparticles.

The selected-area electron diffraction (SAED) pattern was employed to further study the core/shell structure of the nanoparticles. The SAED pattern of Fe_3O_4 nanoparticles can be indexed as Fe_3O_4 (200), (230) and (133) with JCPDS code of 89-6466, and the SAED pattern of Fe_3O_4@Au nanoparticles can be indexed as Fe_3O_4 (122) and (006) with JCPDS code of 89-6466 and Au (311) and (220) with JCPDS code of 89-3697 and 65-2870 (Figure 4.9). Both SAED patterns and TEM images proved the core/shell structure of the Fe_3O_4@Au nanoparticles with the same compositions indicated by XRD patterns.

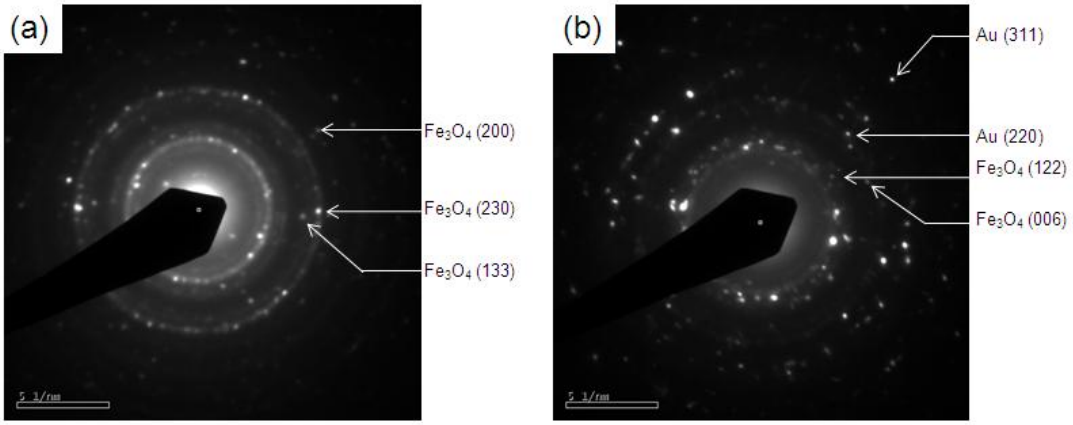

Figure 4.9 SAED patterns of (a) Fe_3O_4 nanoparticles, and (b) Fe_3O_4@Au nanoparticles.

4.1.5 Magnetic Properties of Fe_3O_4 Nanoparticles and Fe_3O_4@Au Nanoparticles

Magnetic properties of the Fe_3O_4 nanoparticles and Fe_3O_4@Au nanoparticles were further characterized by SQUID. According to previous studies,[19] Fe_3O_4 nanoparticles with size smaller than 16 nm show superparamagnetic properties. Superparamagnetic properties of Fe_3O_4 nanoparticles made themselves have potentials in hyperthermia, drug delivery, and most important of all, provide higher contrast enhancement in MR imaging than conventional paramagnetic contrast agents.[74] As shown in Figure 4.10, both the curves of Fe_3O_4 and Fe_3O_4@Au nanoparticles showed similar shape with negligible hysteresis signifying superparamagnetic property. The saturation magnetization (M_s) value of Fe_3O_4 nanoparticles was about 45 emu/g. After being coated by Au shell, the M_s value of the Fe_3O_4@Au nanoparticles decreased to 30 emu/g. The decrease in magnetic saturation for Fe_3O_4@Au nanoparticles can be explained by taking into account the diamagnetic contribution of the intact Au shell layer surrounding the magnetic cores.[75]

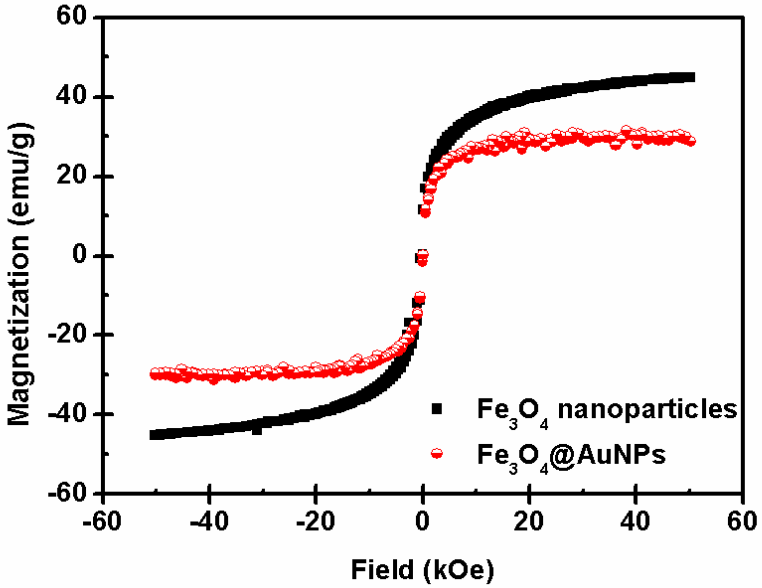

Figure 4.10 Magnetic hysteresis loops of Fe_3O_4 nanoparticles (square) and Fe_3O_4@Au nanoparticles (circle).

4.2 Interaction between DNA Sequences and Doxorubicin

In this study, doxorubicin played roles as both multifunctional anticancer drug and fluorescence agent. In order to quantify doxorubicin, the relationships of concentrations and fluorescence intensity should be illustrated. Figure 4.11 showed the relationships between concentrations and fluorescence intensity of doxorubicin, the linear fitting for the calibration curve is y=0.0235x+3.498, with a correlation coefficient of 0.9931.

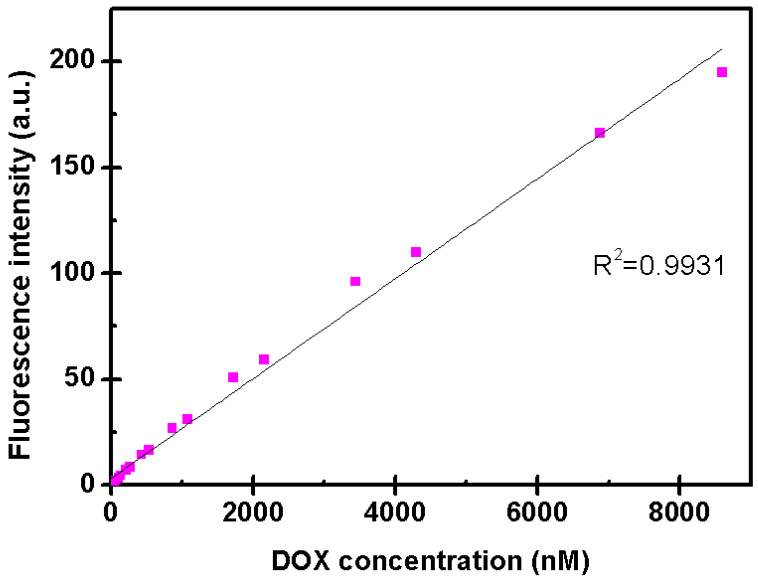

Figure 4.11 Relationships between concentrations and fluorescence intensity of doxorubicin.

Because doxorubicin intercalated preferentially into consecutive –CG– base pairs,[76] the $(CGA)_7$ repeating oligonucleotide was designed, which enhanced doxorubicin-loading capacity, providing binding sites for at least 6-7 doxorubicin molecules. To confirm how many doxorubicin molecules could actually be loaded onto the $(CGA)_7$ oligonucleotides after hybridization with the complementary sequence, 5'-$(TCG)_7$-3', the doxorubicin intercalation by monitoring doxorubicin fluorescence quenching were measured. Although doxorubicin was a fluorescence agent which was excited at 470 nm with emission at 590 nm, the fluorescence can be quenched during its intercalation with DNA.[77] As the amount of added unhybridized (ssDNA) or hybridized (dsDNA) oligonucleotides increased, there was a sequential decrease in the native fluorescence spectrum of doxorubicin that ultimately reached a maximum level of fluorescence quenching (Figure 4.12). Even though the loading capacity of ssDNA and dsDNA showed no significant differences, the dsDNA was

used to carrier the drug in this study. Not only because the structure of double-strand are more stable, but also the planar aromatic chromophore portion of doxorubicin intercalates between two base pairs of double-strand DNA, while the six-membered daunosamine sugar sits in the minor groove and interacts with flanking base pairs immediately adjacent to the intercalation site.[78]

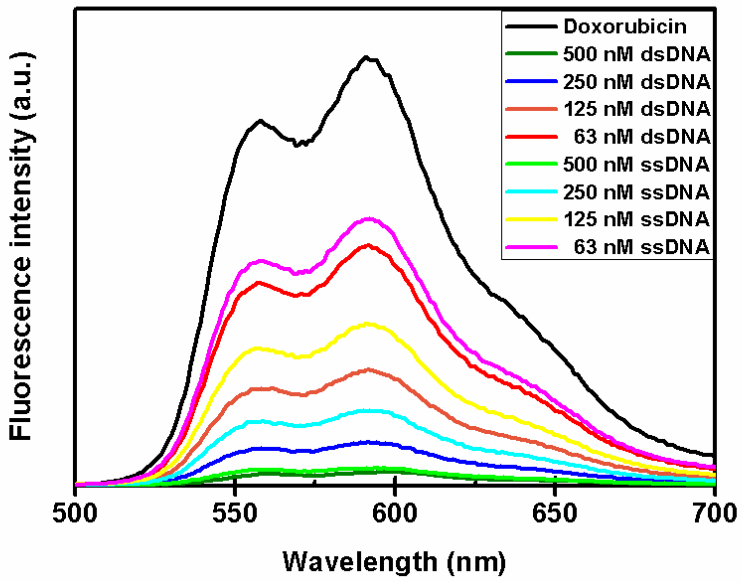

Figure 4.12 Fluorescence spectrum of a doxocrubicin solution (8.6 μM) with increasing concentrations of ssDNA and dsDNA oligonucleotides.

Because the drug delivery was triggered by heat in this study, the variations of doxorubicin and doxorubicin with dsDNA as a function of temperature were monitored by the changes of the fluorescence intensity. First, it must be ensured that the fluorescence will not be influenced in the temperature range for our operation. From Figure 4.13, the fluorescence intensity showed negligible changes at various temperatures. Even at high temperature, the fluorescence intensity of doxorubicin exhibited like those at room temperature, which can be still quantified by fluorescence

intensity. Owing to negligible changes of doxorubicin at any temperatures, the changes of fluorescence intensity of 8.6 μM doxorubicin with 125 nM dsDNA could be explained as the doxorubicin released from the double strand DNA. As shown in Figure 4.14, the higher temperature increased, the higher fluorescence intensity was, meaning the more doxorubicin released. Consequently, it is proved in our experiment that the release of drugs carried by DNA double-helix structure through the feature of dehybridization under heat exposure is realistic.

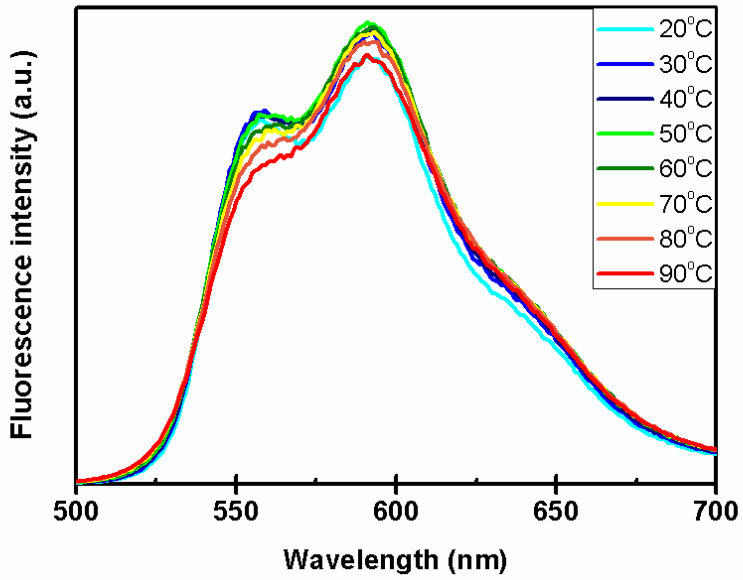

Figure 4.13 Fluorescence spectrum of a doxocrubicin solution (8.6 μM) as a function of temperature.

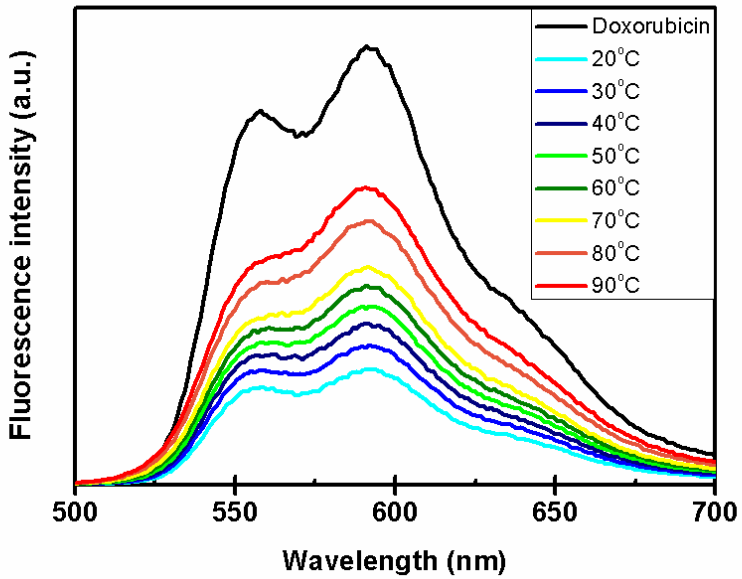

Figure 4.14 Fluorescence spectrum of a doxocrubicin solution (8.6 μM) with 125 nM dsDNA as a function of temperature.

4.3 Fabrication of Drug Carrier—Fe_3O_4@AuNPs-dsDNA-Doxorubicin

After confirming the behavior of doxorubicin and doxorubicin with dsDNA, the $(CGA)_7$ oligonucleotides hybridized with the complementary sequence were modified onto Fe_3O_4@AuNPs by Au-S bond. Because DNA could provide efficient protecting the AuNPs against salinity solutions, the amount of dsDNA required to cover the Fe_3O_4@AuNPs was titrated using NaCl solution to determine the coverage of dsDNA coating the Fe_3O_4@AuNPs.[79] The stability of Fe_3O_4@AuNPs can be monitored by its color with naked eyes. If the dsDNA did not cap the Fe_3O_4@AuNPs completely, the Fe_3O_4@AuNPs aggregated after titrated using NaCl solution, and the color of the Fe_3O_4@AuNPs solution changed from pink to purple. As shown in Figure 4.15, by exploiting interactions between the Fe_3O_4@AuNPs and dsDNA, color changes of the Fe_3O_4@AuNPs could sensitively differentiate the concentration used of dsDNA after

titrating with the salt solution.

The amount of dsDNA and doxorubicin carried by Fe_3O_4@AuNPs was an important parameter for the drug carrying capability of the particle. Therefore, to calculate how many dsDNA were modified onto the Fe_3O_4@AuNPs, excess dsDNA were added into 0.1 mg/mL Fe_3O_4@AuNPs solution for overnight. The unbonded dsDNA were removed by centrifugation and measured. There were 148 nM dsDNA modified onto 0.1 mg/mL Fe_3O_4@AuNPs. In addition, the amount of doxorubicin loaded was 1466 nM per 0.1 mg/mL Fe_3O_4@AuNPs, calculated indirectly by measuring the amount of unloaded doxorubicin remaining after purification of the drug-loaded conjugate by centrifugation. The result suggested that 9-10 doxorubicin molecules were bound by each dsDNA.

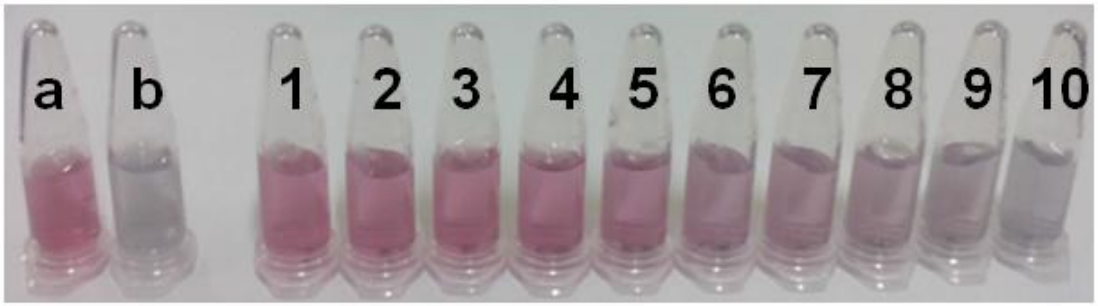

Figure 4.15 Photographic image of (a) Fe_3O_4@AuNPs, (b) Fe_3O_4@AuNPs after adding NaCl solution, and (1)-(10) Fe_3O_4@AuNPs with decreasing concentrations of dsDNA after adding NaCl solution.

In fact, these results were in good agreement with the data obtained from zeta-potential measurement as following. When dsDNA conjugated to Fe_3O_4@AuNPs by Au-S bond, the zeta-potential increased to -27.96 mV, suggesting the charge screening of the DNA, which was similar to previous report.[75] The zeta-potential further increased when doxorubicin loaded onto Fe_3O_4@AuNPs-dsDNA, with the

value of -21.41 mV (Table 2.2), due to the doxorubicin encapsulation and the presence of a positively charged primary amine in doxorubicin structure, respectively.[81]

Sample	Zeta-potential
Fe_3O_4@AuNPs	-52.7 mV
Fe_3O_4@AuNPs bound dsDNA	-27.96 mV
Fe_3O_4@AuNPs-dsDNA conjugated doxorubicin	-21.41 mV

Table 4.2 Zeta-potential of Fe_3O_4@AuNPs, Fe_3O_4@AuNPs bound dsDNA, and Fe_3O_4@AuNPs-dsDNA conjugated doxorubicin.

4.4 Drug Delivery Test

In the compositions of Fe_3O_4@AuNPs-dsDNA-doxorubicin, Fe_3O_4@AuNPs was employed to carry doxorubicin, which played roles as both drug and fluorescence dye, by the thiolated thermo-sensitive dsDNA. When high frequency magnetic field heated the nanoparticles, dsDNA would dehybridize the double strand and release drugs. The stability of Fe_3O_4@AuNPs-dsDNA-doxorubicin at 37^{o}C (an *in vivo* condition) was firstly observed. In the following the drug delivery capability of Fe_3O_4@AuNPs-dsDNA-doxorubicin was tested in various temperatures. At the final step, the drug delivery was controlled by duration time under high frequency magnetic field. All the results were shown in this section.

4.4.1 The Stability of Fe_3O_4@AuNPs-dsDNA-Doxorubicin at 37°C

The stability of Fe_3O_4@AuNPs-dsDNA-doxorubicin at 37°C (an *in vivo* condition) was firstly figured out by observing the doxorubicin non-specific release by diffusion. At beginning, the release rate was gradually increased to 6.69% within 4 hours, then trended mitigating from 4 h to 24 h. After 24 hours, the release rate was fixedly keeping in 20% with slight increasing (Figure 4.16). Non-specific release was one of the causes inducing side effect. Therefore, a low diffusion was significant for drug carrier. As the result, Fe_3O_4@AuNPs-dsDNA-doxorubicin exhibited good stability, and was suitable as a drug carrier.

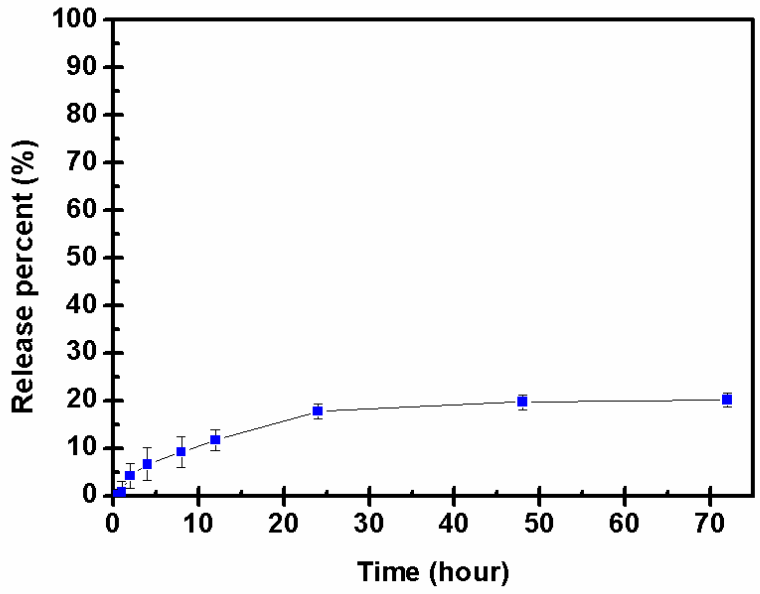

Figure 4.16 The release profile of doxorubicin from doxorubicin-loaded Fe_3O_4@AuNPs-dsDNA by diffusion at 37°C.

4.4.2 Drug Release at Various Temperatures

Because the doxorubicin release was triggered by denaturing of dsDNA, which were themo-sensitive molecules, the drug delivery was examined at various

temperatures. After the doxorubicin loaded Fe_3O_4@AuNPs-dsDNA solution was put in the water bath with different temperature for 10 min to achieve thermal equilibrium, the supernatants of the sample solution were isolated by centrifugation. As can be seen in Figure 4.17, the release rate was lower than 20% when the temperature was lower than 40°C; the results were consistent with the stability test which had the release rate lower than 20% at 37°C. With temperature increasing, the release rate gradually increased. The moderate increasing release rate at 50-70°C should be contributed to the high melting temperature of dsDNA-doxorubicin structure, and the release rate was significant increasing to 68.07% until the temperature reached to 90°C. [82] Consequently, the release rate could be tuned by changing temperature.

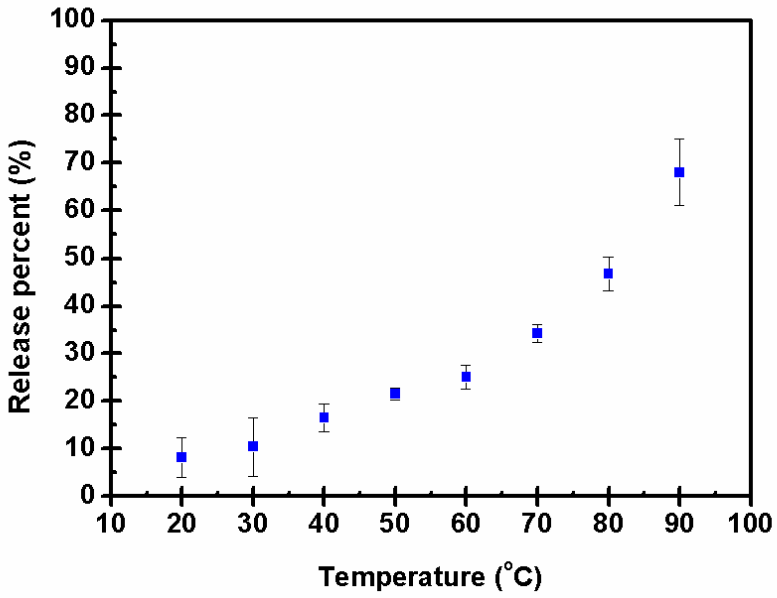

Figure 4.17 Temperature-dependent release profile of doxorubicin from doxorubicin-loaded Fe_3O_4@AuNPs-dsDNA.

4.4.3 Drug Release under High Frequency Magnetic Field

In this study, to achieve magnetic field induced drug release, doxorubicin loaded Fe_3O_4@AuNPs-dsDNA solution was put in the center of the loop of high frequency magnetic field for different time periods. However, the vast majority of drug release research has focused on photothermal release rather than magnetic field induced. To confirm this phenomenon, the heat capability of high frequency magnetic field to magnetic nanoparticles should be figured out.

Typically, the heating phenomenon of magnetic nanoparticles under high frequency field is commonly called hyperthermia; specific loss power (SLP) was used to represent the capability to generate heat from the magnetic coupling between the magnetic moment of nanoparticles and the applied high frequency magnetic field, which was defined as the thermal power dissipation divided by the mass of the magnetic nanoparticles. According to previous study, ferrofluid samples investigated in literature show SLP values of the order 100 W/g.[83] In this experiment, the SLP value was 146 W/g for magnetic Fe_3O_4 nanoparticles, whereas lowered to 111 W/g for magnetic Fe_3O_4@AuNPs at 50 kHz and 8 kA/m. Because the amount of heat generated could be influenced by the properties of the magnetic nanoparticles and the magnetic field parameters. Therefore, at the same magnetic field parameters, the decrease in SLP value for Fe_3O_4@AuNPs can be contributed to the lower saturation magnetization (M_s) value of Fe_3O_4@AuNPs. Nevertheless, Fe_3O_4@AuNPs had similar SLP value to ferrofluid samples investigated in literature, which still led strong possibilities for its use in hyperthermia.

After exposure to high frequency magnetic field at 50 kHz and 8 kA/m, the supernatants of Fe_3O_4@AuNPs-dsDNA-doxorubicin were isolated by centrifugation. The release profile of doxorubicin molecules was quantified by monitoring the increasing fluorescence signals. As shown in Figure 4.18, the fluorescence intensity

increased gradually from 1 min to 7 min, but decreased at 9 min to 15 min. Since the emission could be declined from doxorubicin combining with oligonucleotides, it would be assumed that the contribution of Au-S breaking and released the thiolated strand.[84-85]

From Figure 4.19, with magnetic field inducing for mere 1 minute, the release rate could achieve to 35.76% better than 20% of non-specific release by diffusion, illustrating that magnetic field can actively trigger more drug to release. Furthermore, with different periods of magnetic field inducing, the release rate could be adjusted into various doses. Comparing with the release rate that induced by different temperature water bath, magnetic field could trigger release rate up to 79.8% in less than 10 minutes. Accordingly, the release rate could be tuned by adjusting magnetic field, and the drug could be liberally released in a short time.

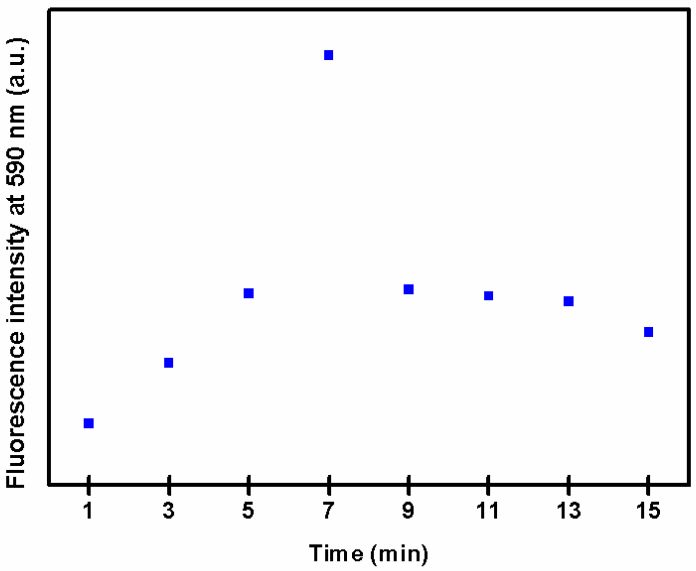

Figure 4.18 The fluorescence intensity of doxorubicin from doxorubicin-loaded Fe_3O_4@AuNPs-dsDNA under high frequency magnetic field for different time periods.

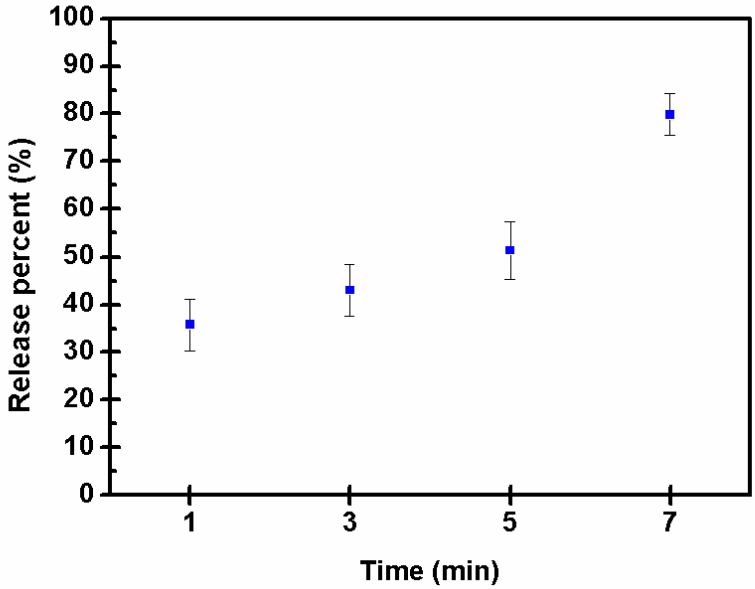

Figure 4.19 The release profile of doxorubicin from doxorubicin-loaded Fe_3O_4@AuNPs-dsDNA under high frequency magnetic field for different time periods.

Chapter 5: Conclusions

In summary, a drug carrier with tunable delivery based on Fe_3O_4 core/Au shell magnetic nanoparticles has been introduced in this study. The Fe_3O_4 core/Au shell nanoparticles were successfully synthesized by a rapid and effective route in aqueous media, and performed an investigation in detail by SEM, TEM, EDS, XRD, SAED, and SQUID. The particles with relatively uniformsize are well-dispersed in solution, and exhibit superparamagnetic property. By conjugating Fe_3O_4@AuNPs with hybridized oligonucleotide which forms a CG-rich duplex that acts as a loading site for the chemo-therapeutic agent doxorubicin, we have constructed a multifunctional nanoparticle that enables tunable drug delivery. By means of adjusting temperature or duration time under high frequency magnetic field, the doxorubicin release varied and the highest dosage could be achieved up to 79%. For future downstream studies, the Fe_3O_4@AuNPs with magnetic cores have potential in MR imaging contrast, and further, by modifying targeting molecules, the Fe_3O_4@AuNPs could perform imaging, targeting, tunable drug delivery simultaneously.

Reference

[1] Eustis, S.; El-Sayed, M. A. Why Gold Nanoparticles Are More Precious than Pretty Gold: Noble Metal Surface Plasmon Resonance and Its Enhancement of the Radiative and Nonradiative Properties of Nanocrystals of Different Shapes. *Chem. Soc. Rev*. **2006**, *35*, 209-217.

[2] Rosi, N. L.; Mirkin, C. A. Nanostructures in Biodiagnostics. *Chem. Rev*. **2005**, *105*, 1547-1562.

[3] Jun, Y. W.; Lee, J. H.; Cheno, J. Chemical Design of Nanoparticle Probes for High-Performance Magnetic Resonance Imaging. *Angew. Chem.-Int. Edit*. **2008**, *47*, 5122-5135.

[4] Niemeyer, C. M. Nanoparticles, Proteins, and Nucleic Acids: Biotechnology Meets Materials Science. *Angew. Chem.-Int. Edit*. **2001**, *40*, 4128-4158.

[5] Katz, E.; Willner, I. Integrated Nanoparticle-Biomolecule Hybrid Systems: Synthesis, Properties, and Applications. *Angew. Chem.-Int. Edit*. **2004**, *43*, 6042-6108.

[6] Whitesides, G. M.; Mathias, J. P.; Seto, C. T. Molecular Self-Assembly and Nanochemistry: A Chemical Strategy for the Synthesis of Nanostructures. *Science* **1991**, *254*, 1312-1319.

[7] Liu, R. R.; Liew, R. S.; Zhou, H.; Xing, B. G. A Simple and Specific Assay for Real-Time Colorimetric Visualization of Beta-Lactamase Activity by Using Gold Nanoparticles. *Angew. Chem.-Int. Edit*. **2007**, *46*, 8799-8803.

[8] Cui, Y.; Wei, Q. Q.; Park, H. K.; Lieber, C. M. Nanowire Nanosensors for Highly Sensitive and Selective Detection of Biological and Chemical Species. *Science* **2001**, *293*, 1289-1292.

[9] Huang, G. S.; Chen, Y. S.; Yeh, H. W. Measuring the Flexibility of

Immunoglobulin by Gold Nanoparticles. *Nano Lett.* **2006**, *6*, 2467-2471.

[10] Bhattacharya, R.; Patra, C. R.; Verma, R.; Kumar, S.; Greipp, P. R.; Mukherjee, P. Gold Nanoparticles Inhibit the Proliferation of Multiple Myeloma Cells. *Adv. Mater.* **2007**, *19*, 711-716.

[11] Tsai, C. Y.; Chang, T. L.; Chen, P. H.; Chen, C. C.; Ko, F. H. Electrical Detection of Protein Using Gold Nanoparticles and Nanogap Electrodes. *Jpn. J. Appl. Phys.* **2007**, *44*, 5711-5716.

[12] Tsai, C. Y.; Chang, T. L.; Chen, C. C.; Ko, F. H.; Chen, P. H. An Ultra Sensitive DNA Detection by Using Gold Nanoparticle Multilayer in Nano-Gap Electrodes. *Microelectron. Eng.* **2005**, *78-79*, 546-555.

[13] LaVan, D. A.; McGuire, T.; Langer, R. Small-Scale Systems for *In Vivo* Drug Delivery. *Nat. Biotechnol.* **2003**, *21*, 1184-1191.

[14] Sarikaya, M.; Tamerler, C.; Jen, A. K. Y.; Schulten, K.; Baneyx, F. Molecular Biomimetics: Nanotechnology through Biology. *Nat. Mater.* **2003**, *2*, 577-585.

[15] Gupta, A. K.; Gupta, M. Synthesis and Surface Engineering of Iron Oxide Nanoparticles for Biomedical Applications. *Biomaterials* **2005**, *26*, 3995-4021.

[16] Lu, A. H.; Salabas, E. L.; Schuth, F. Magnetic Nanoparticles: Synthesis, Protection, Functionalization, and Application. *Angew. Chem.-Int. Edit.* **2007**, *46*, 1222-1244.

[17] Sjogren, C. E.; Brileysaebo, K.; Hanson, M.; Johansson, C. Magnetic Characterization of Iron Oxides for Magnetic Resonance Imaging. *Magn. Reson. Med.* **1994**, *31*, 268-272.

[18] Park, J.; An, K. J.; Hwang, Y. S.; Park, J. G.; Noh, H. J.; Kim, J. Y.; Park, J. H.; Hwang, N. M.; Hyeon, T. Ultra-Large-Scale Syntheses of Monodisperse Nanocrystals. *Nat. Mater.* **2004**, *3*, 891-895.

[19] Sun, S. H.; Zeng, H.; Robinson, D. B.; Raoux, S.; Rice, P. M.; Wang, S. X.; Li, G.

X. Monodisperse MFe_2O_4 (M = Fe, Co, Mn) Nanoparticles. *J. Am. Chem. Soc.* **2004**, *126*, 273-279.

[20] Jana, N. R.; Chen, Y. F.; Peng, X. G. Size- and Shape-Controlled Magnetic (Cr, Mn, Fe, Co, Ni) Oxide Nanocrystals via a Simple and General Approach. *Chem. Mat.* **2004**, *16*, 3931-3935.

[21] Langevin, D. Micelles and Microemulsions. *Annu. Rev. Phys. Chem*. **1992**, *43*, 341-369.

[22] Wang, X.; Zhuang, J.; Peng, Q.; Li, Y. D. A General Strategy for Nanocrystal Synthesis. *Nature* **2005**, *437*, 121-124.

[23] Babes, L.; Denizot, B.; Tanguy, G.; Jeune, J. J.; Jallet, P. Synthesis of Iron Oxide Nanoparticles Used as MRI Contrast Agents: A Parametric Study. *J. Colloid Interface Sci*. **1999**, *212*, 474-482.

[24] Goya, G. F.; Berquo, T. S.; Fonseca, F. C.; Morales, M. P. Static and Dynamic Magnetic Properties of Spherical Magnetite Nanoparticles. *J. Appl. Phys.* **2003**, *94*, 3520-3528.

[25] Sun, C.; Lee, J. S. H.; Zhang, M. Q. Magnetic Nanoparticles in MR Imaging and Drug Delivery. *Adv. Drug Deliv. Rev*. **2008**, *60*, 1252-1265.

[26] Jun, Y. W.; Lee, J. H.; Cheon, J. Chemical Design of Nanoparticle Probes for High-Performance Magnetic Resonance Imaging. *Angew. Chem.-Int. Edit.* **2008**, *47*, 5122-5135.

[27] Chouly, C.; Pouliquen, D.; Lucet, I.; Jeune, J. J.; Jallet, P. Development of Superparamagnetic Nanoparticles for MRI: Effect of Particle Size, Charge and Surface Nature on Biodistribution. *J. Microencapsul.* **1996**, *13*, 245-255.

[28] Davis, M. E.; Chen, Z.; Shin, D. M. Nanoparticle Therapeutics: An Emerging Treatment Modality for Cancer. *Nat. Rev. Drug Discov*. **2008**, *7*, 771-782.

[29] Namdeo, M.; Saxena, S.; Tankhiwale, R.; Bajpai, M.; Mohan, Y. M.; Bajpai, S. K.

Magnetic Nanoparticles for Drug Delivery Applications. *J. Nanosci. Nanotechnol.* **2008**, *8*, 3247-3271.

[30] Veiseh, O.; Gunn, J. W.; Zhang, M. Q. Design and Fabrication of Magnetic Nanoparticles for Targeted Drug Delivery and Imaging. *Adv. Drug Deliv. Rev*. **2010**, *62*, 284-304.

[31] Storm, G.; Belliot, S. O.; Daemen, T.; Lasic, D. D. Surface Modification of Nanoparticles to Oppose Uptake by the Mononuclear Phagocyte System. *Adv. Drug Deliv. Rev*. **1995**, *17*, 31-48.

[32] Kohler, N.; Sun, C.; Wang, J.; Zhang, M. Q. Methotrexate-Modified Superparamagnetic Nanoparticles and Their Intracellular Uptake into Human Cancer Cells. *Langmuir* **2005**, *21*, 8858-8864.

[33] Kohler, N.; Sun, C.; Fichtenholtz, A.; Gunn, J.; Fang, C.; Zhang, M. Q. Methotrexate-Immobilized Poly(ethylene glycol) Magnetic Nanoparticles for MR Imaging and Drug Delivery. *Small* **2006**, *2*, 785-792.

[34] Schulze, K.; Koch, A.; Schopf, B.; Petri, A.; Steitz, B.; Chastellain, M.; Hofmann, M.; Hofmann, H.; von Rechenberg, B. Intraarticular Application of Superparamagnetic Nanoparticles and Their Uptake by Synovial Membrane—An Experimental Study in Sheep. *J. Magn. Magn. Mater*. **2005**, *293*, 419-432.

[35] Jain, T. K.; Morales, M. A.; Sahoo, S. K.; Leslie-Pelecky, D. L.; Labhasetwar, V. Iron Oxide Nanoparticles for Sustained Delivery of Anticancer Agents. *Mol. Pharm*. **2005**, *2*, 194-205.

[36] Huh, Y. M.; Jun, Y. W.; Song, H. T.; Kim, S.; Choi, J. S.; Lee, J. H.; Yoon, S.; Kim, K. S.; Shin, J. S.; Suh, J. S.; Cheon, J. *In Vivo* Magnetic Resonance Detection of Cancer by Using Multifunctional Magnetic Nanocrystals. *J. Am. Chem. Soc*. **2005**, *127*, 12387-12391.

[37] Kute, T.; Lack, C. M.; Willingham, M.; Bishwokama, B.; Williams, H.; Barrett,

K.; Mitchell, T.; Vaughn, J. P. Development of Herceptin Resistance in Breast Cancer Cells. *Cytom. Part A* **2004**, *57A*, 86-93.

[38] Ito, A.; Kuga, Y.; Honda, H.; Kikkawa, H.; Horiuchi, A.; Watanabe, Y.; Kobayashi, T. Magnetite Nanoparticle-Loaded Anti-HER2 Immunoliposomes for Combination of Antibody Therapy with Hyperthermia. *Cancer Lett*. **2004**, *212*, 167-175.

[39] Brigger, I.; Dubernet, C.; Couvreur, P. Nanoparticles in Cancer Therapy and Diagnosis. *Adv. Drug Deliv. Rev*. **2002**, *54*, 631-651.

[40] Juliano, R. L.; Alahari, S.; Yoo, H.; Kole, R.; Cho, M. Antisense Pharmacodynamics: Critical Issues in the Transport and Delivery of Antisense Oligonucleotides. *Pharm. Res*. **1999**, *16*, 494-592.

[41] Scherer, F.; Anton, M.; Schillinger, U.; Henkel, J.; Bergemann, C.; Kruger, A.; Gansbacher, B.; Plank, C. Magnetofection: Enhancing and Targeting Gene Delivery by Magnetic Force *In Vitro* and *In Vivo*. *Gene Ther*. **2002**, *9*, 102-109.

[42] Krotz, F.; de Wit, C.; Sohn, H. Y.; Zahler, S.; Gloe, T.; Pohl, U.; Plank, C. Magnetofection—A Highly Efficient Tool for Antisense Oligonucleotide Delivery *In Vitro* and *In Vivo*. *Mol. Ther*. **2003**, *7*, 700-710.

[43] Dobson, J. Gene Therapy Progress and Prospects: Magnetic Nanoparticle-Based Gene Delivery. *Gene Ther*. **2006**, *13*, 283-287.

[44] Pan, B. F.; Cui, D. X.; Sheng, Y.; Ozkan, C. G.; Gao, F.; He, R.; Li, Q.; Xu, P.; Huang, T. Dendrimer-Modified Magnetic Nanoparticles Enhance Efficiency of Gene Delivery System. *Cancer Res*. **2007**, *67*, 8156-8163.

[45] Jordan, A.; Scholz, R.; Wust, P.; Fahling, H.; Felix, R. Magnetic Fluid Hyperthermia (MFH): Cancer Treatment with AC Magnetic Field Induced Excitation of Biocompatible Superparamagnetic Nanoparticles. *J. Magn. Magn. Mater*. **1999**, *201*, 413-419.

[46] Moroz, P.; Jones, S. K.; Gray, B. N. Magnetically Mediated Hyperthermia: Vurrent Status and Future Directions. *Int. J. Hyperthermia* **2002**, *18*, 267-284.

[47] Jordan, A.; Wust, P.; Fahling, H.; John, W.; Hinz, A.; Felix, R. Inductive Heating of Ferrimagnetic Particles and Magnetic Fluids: Physical Evaluation of Their Potential for Hyperthermia. *Int. J. Hyperthermia* **2009**, *25*, 499-511.

[48] Gonzales-Weimuller, M.; Zeisberger, M.; Krishnan, K. M. Size-Dependant Heating Rates of Iron Oxide Nanoparticles for Magnetic Fluid Hyperthermia. *J. Magn. Magn. Mater.* **2009**, *321*, 1947-1950.

[49] Shliomis, M. I.; Pshenichnikov, A. F.; Morozov, K. I.; Shurubor, I. Y. Magnetic-Properties of Ferrocolloids. *J. Magn. Magn. Mater.* **1990**, *85*, 40-46.

[50] Fortin, J. P.; Wilhelm, C.; Servais, J.; Menager, C.; Bacri, J. C.; Gazeau, F. Size-Sorted Anionic Iron Oxide Nanomagnets as Colloidal Mediators for Magnetic Hyperthermia. *J. Am. Chem. Soc.* **2007**, *129*, 2628-2635.

[51] Laurent, S.; Forge, D.; Port, M.; Roch, A.; Robic, C.; Elst, L. V.; Muller, R. N. Magnetic Iron Oxide Nanoparticles: Synthesis, Stabilization, Vectorization, Physicochemical Characterizations, and Biological Applications. *Chem. Rev.* **2008**, *108*, 2064-2110.

[52] Reiss, P.; Bleuse, J.; Pron, A. Highly Luminescent CdSe/ZnSe Core/Shell Nanocrystals of Low Size Dispersion. *Nano Lett.* **2002**, *2*, 781-784.

[53] Cao, Y. W.; Jin, R.; Mirkin, C. A. DNA-Modified Core-Shell Ag/Au Nanoparticles. *J. Am. Chem. Soc.* **2001**, *123*, 7961-7962.

[54] Wang, D. S.; He, J. B.; Rosenzweig, N.; Rosenzweig, Z. Superparamagnetic Fe_2O_3 Beads-CdSe/ZnS Quantum Dots Core-Shell Nanocomposite Particles for Cell Separation. *Nano Lett.* **2004**, *4*, 409-413.

[55] Kellogg, G. E.; Scarsdale, J. N.; Fornari, F. A. Identification and Hydropathic Characterization of Structural Features Affecting Sequence Specificity for

Doxorubicin Intercalation into DNA Double-Stranded Polynucleotides. *Nucleic Acids Res.* **1998**, *26*, 4721-4732.

[56] Bailly, C.; Suh, D.; Waring, M. J.; Chaires, J. B. Binding of Daunomycin to Diaminopurine- and/or Inosine-Substituted DNA. *Biochemistry* **1998**, *37*, 1033-1045.

[57] http://www.ntuh.gov.tw/phr/intergrate.aspx

[58] O'Brien, M. E. R.; Wigler, N.; Inbar, M.; Rosso, R.; Grischke, E.; Santoro, A.; Catane, R.; Kieback, D. G.; Tomczak, P.; Ackland, S. P.; Orlandi, F.; Mellars, L.; Alland, L.; Tendler, C. Reduced Cardiotoxicity and Comparable Efficacy in a Phase III Trial of Pegylated Liposomal Doxorubicin HCl (CAELYX™/Doxil®) versus Conventional Doxorubicin for First-Line Treatment of Metastatic Breast Cancer. *Ann. Oncol.* **2004**, *15*, 440-449.

[59] http://en.wikipedia.org/wiki/XRD

[60] http://en.wikipedia.org/wiki/Energy-dispersive_X-ray_spectroscopy

[61] Lyon, J. L.; Fleming, D. A.; Stone, M. B.; Schiffer, P.; Williams, M. E. Synthesis of Fe Oxide Core/Au Shell Nanoparticles by Iterative Hydroxylamine Seeding. *Nano Lett.* **2004**, *4*, 719-723.

[62] Creighton, J. A.; Eadon, D. G. Ultraviolet Visible Absorption-Spectra of the Colloidal Metallic Elements. *J. Chem. Soc., Faraday Trans.* **1991**, *87*, 3881-3891.

[63] Jensen, T. R.; Malinsky, M. D.; Haynes, C. L.; Van Duyne, R. P. Nanosphere Lithography: Tunable Localized Surface Plasmon Resonance Spectra of Silver Nanoparticles. *J. Phys. Chem. B* **2000**, *104*, 10549-10556.

[64] Mulvaney, P. Surface Plasmon Spectroscopy of Nanosized Metal Particles. *Langmuir* **1996**, *12*, 788-800.

[65] Xu, M. L.; Dignam, M. J. A New Approach to the Surface Plasma Resonance of Small Metal Particles. *J. Chem. Phys.* **1992**, *96*, 3770-3778.

[66] Jensen, T. R.; Duval, M. L.; Kelly, K. L.; Lazarides, A. A.; Schatz, G.C.; Van

Duyne, R. P. Nanosphere Lithography: Effect of the External Dielectric Medium on the Surface Plasmon Resonance Spectrum of a Periodic Array of Sliver Nanoparticles. *J. Phys. Chem. B* **1999**, *103*, 9846-9853.

[67] Underwood, S.; Mulvaney, P. Effect of the Solution Refractive-Index on the Color of Gold Colloids. *Langmuir* **1994**, *10*, 3427-3430.

[68] Templeton, A. C.; Pietron, J. J.; Murray, R. W.; Mulvaney, P. Solvent Refractive Index and Core Charge Influences on the Surface Plasmon Absorbance of Alkanethiolate Monolayer-Protected Gold Clusters. *J. Phys. Chem. B* **2000**, *104*, 564-570.

[69] Haiss, W.; Thanh, N. T. K.; Aveyard, J.; Fernig, D. G. Determination of Size and Concentration of Gold Nanoparticles from UV-Vis Spectra. *Anal. Chem.* **2007**, *79*, 4215-4221.

[70] Pang, L. L.; Li, J. S.; Jiang, J. H.; Le, Y.; Shen, G. L.; Yu, R. Q. A Novel Detection Method for DNA Point Mutation Using QCM Based on Fe_3O_4/Au Core/Shell Nanoparticle and DNA Ligase Reaction. *Sens. Actuator B-Chem.* **2007**, *127*, 311-316.

[71] Lu, Z. Y.; Wang, G.; Zhuang, J. Q.; Yang, W. S. Effects of the Concentration of Tetramethylammonium Hydroxide Peptizer on the Synthesis of Fe_3O_4/SiO_2 Core/Shell Nanoparticles. *Colloid Surf. A-Physicochem. Eng. Asp.* **2006**, *278*, 140-143.

[72] Choi, H. S.; Liu, W.; Misra, P.; Tanaka, E.; Zimmer, J. P.; Ipe, B. I.; Bawendi, M. G.; Frangioni, J. V. Renal Clearance of Quantum Dots. *Nat. Biotechnol.* **2007**, *25*, 1165-1170.

[73] Veiseh, O.; Gunn, J. W.; Zhang, M. Q. Design and Fabrication of Magnetic Nanoparticles for Targeted Drug Delivery and Imaging. *Adv. Drug Deliv. Rev.* **2010**, *62*, 284-304.

[74] Lee, H.; Lee, E.; Kim, D. K.; Jang, N. K.; Jeong, Y. Y.; Jon, S. Antibiofouling Polymer-Coated Superparamagnetic Iron Oxide Nanoparticles as Potential Magnetic Resonance Contrast Agents for *In Vivo* Cancer Imaging. *J. Am. Chem. Soc.* **2006**, *128*, 7383-7389.

[75] Zhou, X.; Xu, W. L.; Wang, Y.; Kuang, Q.; Shi, Y. F.; Zhong, L. B.; Zhang, Q. Q. Fabrication of Cluster/Shell Fe_3O_4/Au Nanoparticles and Application in Protein Detection via a SERS Method. *J. Phys. Chem. C* **2010**, *114*, 19607-19613.

[76] Chaires, J. B.; Herrera, J. E.; Waring, M. J. Preferential Binding of Daunomycin to 5'ATCG and 5'ATGC Sequences Revealed by Footprinting Titration Experiments. *Biochemistry* **1990**, *29*, 6145-6153.

[77] Venne, A.; Li, S. M.; Mandeville, R.; Kabanov, A.; Alakhov, V. Hypersensitizing Effect of Pluronic L61 on Cytotoxic Activity, Transport, and Subcellular Distribution of Doxorubicin in Multiple Drug-Resistant Cells. *Cancer Res.* **1996**, *56*, 3626-3629.

[78] Frederick, C. A.; Williams, L. D.; Ughetto, G.; Vandermarel, G. A.; Vanboom, J. H.; Rich, A.; Wang, A. H. J. Structural Comparison of Anticancer Drug DNA Complexes: Adriamycin and Daunomycin. *Biochemistry* **1990**, *29*, 2538-2549.

[79] Chithrani, B. D.; Ghazani, A. A.; Chan, W. C. W. Determining the Size and Shape Dependence of Gold Nanoparticle Uptake into Mammalian Cells. *Nano Lett.* **2006**, *6*, 662-668.

[80] Park, S.; Hamad-Schifferli, K. Evaluation of Hydrodynamic Size and Zeta-Potential of Surface-Modified Au Nanoparticle-DNA Conjugates via Ferguson Analysis. *J. Phys. Chem. C* **2008**, *112*, 7611-7616.

[81] Yoo, H. S.; Lee, K. H.; Oh, J. E.; Park, T. G. *In Vitro* and *In Vivo* Anti-Tumor Activities of Nanoparticles Based on Doxorubicin-PLGA Conjugates. *J. Control. Release* **2000**, *68*, 419-431.

[82] Alexander, C. M.; Maye, M. M.; Dabrowiak, J. C. DNA-Capped Nanoparticles

Designed for Doxorubicin Drug Delivery. *Chem. Commun.* **2011**, *47*, 3418-3420.

[83] Martinez-Boubeta, C.; Balcells, L.; Cristofol, R.; Sanfeliu, C.; Rodriguez, E.; Weissleder, R.; Lope-Piedrafita, S.; Simeonidis, K.; Angelakeris, M.; Sandiumenge, F.; Calleja, A.; Casas, L.; Monty, C.; Martinez, B. Self-Assembled Multifunctional Fe/MgO Nanospheres for Magnetic Resonance Imaging and Hyperthermia. *Nanomed.-Nanotechnol. Biol. Med.* **2010**, *6*, 362-370.

[84] Poon, L.; Zandberg, W.; Hsiao, D.; Erno, Z.; Sen, D.; Gates, B. D.; Branda, N. R. Photothermal Release of Single-Stranded DNA from the Surface of Gold Nanoparticles Through Controlled Denaturating and Au-S Bond Breaking. *ACS Nano* **2010**, *4*, 6395-6403.

[85] Jain, P. K.; Qian, W.; El-Sayed, M. A. Ultrafast Cooling of Photoexcited Electrons in Gold Nanoparticle-Thiolated DNA Conjugates Involves the Dissociation of the Gold-Thiol Bond. *J. Am. Chem. Soc.* **2006**, *128*, 2426-2433.